

# Chapter 4

## Structure–Function of IBPs and Their Interactions with Ice



Maya Bar-Dolev, Koli Basu, Ido Braslavsky, and Peter L. Davies

### 4.1 Introduction

One of the key factors in understanding how a protein functions is to know its three-dimensional (3-D) structure at atomic resolution. In many cases, the protein structure provides enough clues to deduce its mechanism of action. Yet in the case of ice-binding proteins (IBPs), although high resolution structures of some IBPs were experimentally determined over two decades ago, their interactions with ice, their natural ligand, is still a matter of debate and extensive research. After the three-dimensional structure of type I AFP from flounder was published in 1988 (Yang et al. 1988), many experimental and theoretical studies were conducted to elucidate its ice-binding site (IBS) and find out how it adheres to ice at the molecular level. The publication of other AFP structures, and the discovery of AFPs in other biological kingdoms, have increased interest in understanding the driving force for ice recognition and the crucial elements involved in freezing point depression. The mystery of protein–ice interactions results from several issues. One is the ambiguity of the interface between ice and water, which makes the ligand difficult to define at the molecular level (Guo et al. 2012; Vance et al. 2014). Another is that the difference between bulk water and ice, the ligand, is only in the spatial organization of the water molecules. These aspects make ice recognition a challenging issue to unravel. Another complication lies in the diversity of IBPs structures and functions, making it difficult to formulate generalized conclusions. This chapter describes the structural diversity of IBPs with emphasis on the structures of the IBSs and their specificities

---

M. Bar-Dolev · I. Braslavsky  
The Hebrew University of Jerusalem, Rehovot, Israel  
e-mail: [maya.bar1@mail.huji.ac.il](mailto:maya.bar1@mail.huji.ac.il); [ido.braslavsky@mail.huji.ac.il](mailto:ido.braslavsky@mail.huji.ac.il)

K. Basu · P. L. Davies (✉)  
Queen's University, Kingston, ON, Canada  
e-mail: [0kb15@queensu.ca](mailto:0kb15@queensu.ca); [peter.davies@queensu.ca](mailto:peter.davies@queensu.ca)




for different planes of ice. The topics of ice shaping under different temperature regimes, which is a consequence of IBP specificities for different ice planes, the effects of protein size on activity, and protein engineering studies on IBPs are presented. We discuss the opposing functions of ice-nucleating proteins (INPs) and AFPs in the context of the structural differences between these proteins. Furthermore, we explain the interactions of IBPs with water and ice at the molecular level with emphasis on recent theories about the importance of the hydration shell, the anchored clathrate water mechanism, the issue of reversible/irreversible binding, and dynamic aspects of ice binding by different types of IBPs.

The term “ice-binding proteins” is used in this chapter to embrace all proteins that bind ice. These include those that function as freezing point depressors (AFPs) and others such as ice-recrystallization inhibitors, INPs, and ice adhesins.

## 4.2 Structural Diversity of IBPs

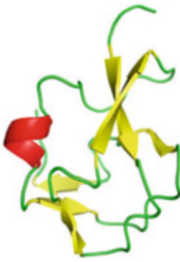
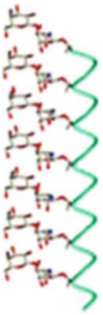
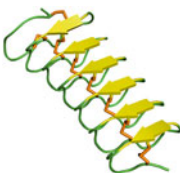
IBP structures are incredibly diverse considering they all share the same function of binding to ice (Davies 2014). That their primary and tertiary structures are radically different attests to the fact that they have evolved on many separate occasions from different progenitors in various branches of the tree of life (Bar Dolev et al. 2016b) (discussed in detail in Chap. 9 of Vol. 1). The structures of fish type I, II, and III AFPs as well as some of the insect and plant IBPs have been described in detail and extensively reviewed (Bar Dolev et al. 2016b; Davies 2014; Duman 2001; Feeney et al. 1986; Venketesh and Dayananda 2008). Some branches (like arthropods, plants, and bacteria) have only been sparsely surveyed for ice-binding activity, and the likelihood of new IBP structures being found here is high. IBPs are typically small, single-domain proteins, the majority of which are repetitive in structure. Details of solved and convincingly modeled IBP 3-D structures are presented in Table 4.1. These include the three types of AFPs found in fish: short (3–4 kDa)  $\alpha$ -helical type I AFPs that have independently arisen four times in fishes (Graham et al. 2013), as well as a long-type I AFP dimer that folds into a four-helix bundle (Maxi), and the globular type II and type III AFPs. Several types of  $\beta$ -solenoid IBPs are found in insects, plants, and microorganisms, and a polyproline type II helix bundle has been described in snow fleas (Collembola), a primitive arthropod. The IBP DUF3494 fold, which is widely dispersed in microorganisms due to lateral gene transfer (Raymond and Kim 2012), has a discontinuous  $\beta$ -solenoid with a supporting  $\alpha$ -helix (see Table 4.1). Additional IBPs have been modeled with high confidence (Basu et al. 2015; Lin et al. 2011). The regularity of repeating structures might facilitate interaction with a crystal lattice and help explain the frequent evolution of the beta-solenoid fold in IBPs. IBPs function at 0 °C or lower. A few of them rely almost entirely on hydrogen bonding for the stability of their folds (see snow flea and type I AFPs in Table 4.1) and are easily denatured by warming to room temperature. Some IBPs are stabilized by disulfide bridges, like type II AFP and the AFP from the insect *Tenebrio molitor* (TmAFP), and some by coordinating  $\text{Ca}^{2+}$  ions, like type II

**Table 4.1** Structures and main properties of IBPs

Name and structure	Details
<p>Type I AFP</p>  <p>PDB: 1wfa</p>	<p><i>Organisms:</i> Several branches of fishes: righteye flounders (Duman and DeVries 1976; Knight et al. 1991), sculpins (Hew et al. 1985; Low et al. 2001), snailfish (Evans and Fletcher 2001), cunner (Hobbs et al. 2011).  <i>Structure:</i> Amphipathic <math>\alpha</math>-helix with 50–65% Ala. Despite apparent homology based on Ala-richness, type I AFPs have independently evolved on at least four occasions (Graham et al. 2013). The helix has an 11-residue periodicity, with 3.7 aa/turn. Size: <math>\sim 55 \times 6 \times 6 \text{ \AA}</math>.  <i>Isoforms:</i> Many, including tissue-specific. Most are 33–42 aa peptides.  <i>IBS:</i> Involves the indicated Thr and Ala in TxxxAxxxAxx repeats that project on one side of the helix.  <i>Ice planes:</i> Flounder and plaice AFPs bind to the <math>[2\bar{0}21]</math> pyramidal plane. Sculpin AFP binds to the <math>[11\bar{2}0]</math> secondary prism plane.  <i>Activity:</i> Moderate TH activity. Produce bipyramidal ice shapes with a constant <math>a:c</math> axis ratio of 3.3 (Wen and Laursen 1992b).</p>
<p>Long type I AFP, Maxi</p> 	<p><i>Organisms:</i> Winter flounder (Sun et al. 2014).  <i>Structure:</i> A four-helix bundle homodimer. Each <math>\alpha</math>-helix monomer has a hairpin fold and the two hairpins align in an antiparallel fashion. The two helices are homologous to type I AFP but 5 times longer. Size: <math>\sim 145 \times 20 \times 20 \text{ \AA}</math>.  <i>Isoforms:</i> (Short) type I AFP.  <i>IBS:</i> Ice-like waters organized by the aqueous core extend to the protein surface between the helices.  <i>Ice planes:</i> Multiple including the basal plane.  <i>Activity:</i> Hyperactive.</p>
<p>Type II AFP</p>  <p>PDB: 2py2</p>	<p><i>Organisms:</i> Several species of fish; sea raven (Patel and Graether 2010), rainbow and Japanese smelt (Yamashita et al. 2003), herring (Ewart and Fletcher 1990) (Liu et al. 2007), longsnout poacher (Nishimiya et al. 2008).  <i>Structure:</i> 14–24 kDa globular protein with a C-type lectin fold. Contains five disulfide bonds. Occurs as <math>\text{Ca}^{2+}</math>-dependent and -independent forms. The protein forms a dimer in rainbow smelt (Achenbach and Ewart 2002). Size: <math>\sim 30 \times 30 \times 40 \text{ \AA}</math>.  <i>Isoforms:</i> Many, including organ-specific (Liu et al. 2007).  <i>IBS:</i> Ill-defined. In the <math>\text{Ca}^{2+}</math>-dependent type II AFPs the metal ion is part of the ice-binding site (Liu et al. 2007), but neighboring regions of the protein are also involved in ice binding (Loewen et al. 1998).  <i>Ice planes:</i> Non-basal.  <i>Activity:</i> Produces bipyramidal ice shapes and has moderate TH activity.</p>

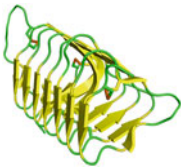
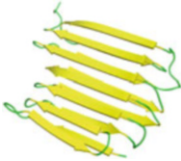


(continued)

**Table 4.1** (continued)

Name and structure	Details
<p>Type III AFP</p>  <p>PDB: 5MSI</p>	<p><i>Organisms:</i> Several families of fishes from one suborder; e.g., ocean pout (Li et al. 1985) and other eelpouts (Cheng and DeVries 1989).</p> <p><i>Structure:</i> 7 kDa, Globular and rigid with short imperfect <math>\beta</math>-strands and a single-helix turn (Jia et al. 1996). Size: <math>\sim 30 \times 20 \times 20 \text{ \AA}</math>.</p> <p><i>Isoforms:</i> Numerous with 50% identity (Hew et al. 1988; Nishimiya et al. 2005).</p> <p>A dimer (Wilkins et al. 2014) and a natural tandem repeat have been seen (Wang et al. 1995).</p> <p><i>IBS:</i> Compound. Two adjacent ice-binding surfaces lie inclined to each other and bind different ice planes (Garnham et al. 2010).</p> <p><i>Ice planes:</i> Several—including primary prism plane [10<math>\bar{1}</math>0], pyramidal [20<math>\bar{2}</math>1], and perhaps some additional planes inclined by a small rotation from these planes (Antson et al. 2001).</p> <p><i>Activity:</i> QAE isoforms have moderate TH activity. SP isoforms shape ice but only stop it growing in the presence of the QAE isoforms (Nishimiya et al. 2005). Produce bypyramidal ice shapes with varying <i>a:c</i> axis ratios (DeLuca et al. 1996).</p>
<p>AFGPs</p>  <p>(Jia and Davies 2002)</p>	<p><i>Organisms:</i> Two distinct branches of fishes: Antarctic toothfish (DeVries and Wohlschlag 1969) and cods (Chen et al. 1997).</p> <p><i>Structure:</i> From 4 to 50 repeats of the TA/PA tripeptide with all hydroxyl groups of the threonines glycosylated by the disaccharide 3-<i>O</i>-(<math>\beta</math>-D-galactosyl)-(<math>\alpha</math>1 <math>\rightarrow</math> 3)-<i>N</i>-acetylglucosamine. Produced from much larger polyproteins. Most likely fold as an amphipathic helix of the PPII type (Tachibana et al. 2004)</p> <p><i>Isoforms:</i> In the rock cod (<i>Gadus ogac</i>) the AFGP isoforms range in size from 2.6 to 24 kDa as measured by electrospray mass spectrometry (Wu et al. 2001).</p> <p><i>IBS:</i> unknown.</p> <p><i>Planes bound:</i> Primary prism planes (Knight et al. 1993).</p> <p><i>Activity:</i> Low TH activity for the smallest isoforms; moderate activity for the longer isoforms.</p>
<p><i>Tm</i>AFP</p>  <p>PDB: 1EZG</p>	<p><i>Organisms:</i> Insect. Yellow mealworm (<i>Tenebrio molitor</i>) (Graham et al. 1997; Liou et al. 2000), pyrochid beetle (<i>Dendroides Canadensis</i>) (Duman et al. 1998).</p> <p><i>Structure:</i> 8–9 kDa, tight <math>\beta</math>-solenoid with a rectangular cross section. The coils are composed of the tandem 12-aa repeat sequence TCTX<math>\text{SXXCXXAX}</math>. Eight disulfide bonds cross-link the coils and rigidify the structure that lacks a hydrophobic core (Liou et al. 2000). Most isoforms contain a consensus <i>N</i>-glycosylation site near the C-terminus (nonessential for activity and folding) (Liou et al. 1999).</p> <p>Size: <math>\sim 32 \times 14 \times 12 \text{ \AA}</math>.</p> <p><i>Isoforms:</i> Many. Most have 7 coils; a few have 8–11 coils (84–120 aa) (Liou et al. 1999).</p> <p><i>IBS:</i> A flat <math>\beta</math>-sheet with regularly spaced Thr-Cys-Thr motifs (Liou et al. 2000).</p> <p><i>Planes bound:</i> Multiple, including basal (Bar Dolev et al. 2016b; Scotter et al. 2006).</p> <p><i>Activity:</i> High TH (hyperactive). Produce lemon-shaped ice crystals.</p>

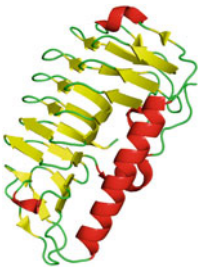
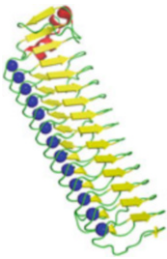
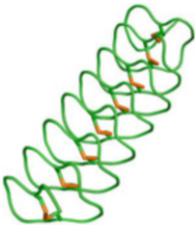
(continued)

**Table 4.1** (continued)

Name and structure	Details
sbwAFP  PDB: 1M8N	<p><b>Organisms:</b> Insect. Spruce budworm (<i>Choristoneura fumiferana</i>) (Graether et al. 2000).</p> <p><b>Structure:</b> 9–12.5 kDa, tight <math>\beta</math>-solenoid of <math>\sim</math>15-residue coils with a triangular cross section and a TXT motif. 4–5 inter-stand disulfide bonds. Size: <math>\sim</math>36 <math>\times</math> 20 <math>\times</math> 18 Å.</p> <p><b>Isoforms:</b> Several with 5 or 7 repeats, in some there are 16 or 17 aa/coil (Doucet et al. 2000).</p> <p><b>IBS:</b> Flat <math>\beta</math>-sheet of TXT motifs (Graether et al. 2000).</p> <p><b>Planes bound:</b> Primary prism plane and basal plane (Graether et al. 2000; Pertaya et al. 2008).</p> <p><b>Activity:</b> High TH (hyperactive). Produces flat-tipped, hexagonal-shaped ice crystals (Graether et al. 2000; Pertaya et al. 2008).</p>
RiAFP  PDB: 4DT5	<p><b>Organisms:</b> Insect. <i>Rhagium inquisitor</i> (Hakim et al. 2013) and longhorn beetle <i>Rhagium mordax</i> (Kristiansen et al. 2011, 2012).</p> <p><b>Structure:</b> 13 kDa, Flat <math>\beta</math>-sandwich with a rectangular cross section. The structure consists of 7 loops of 13–20 aa making two staggered <math>\beta</math>-sheets 6 Å apart, with Ser and Ala side-chains interdigitating inside, making the tight packing similar to silk fibers, without a hydrophobic core. One S–S bond (Hakim et al. 2013). Size: <math>\sim</math>35 <math>\times</math> 30 <math>\times</math> 6 Å.</p> <p><b>Isoforms:</b> Five isoforms with the same number of loops in the beetle <i>Rhagium mordax</i> (Kristiansen et al. 2011, 2012).</p> <p><b>IBS:</b> Predicted to be one of the two <math>\beta</math>-sheets, which is composed of an array of five expanded strands of the motif TXTTXT (Hakim et al. 2013).</p> <p><b>Planes bound:</b> Multiple, including primary prism and basal planes (Hakim et al. 2013)</p> <p><b>Activity:</b> High TH (hyperactive).</p>
sfAFP PDB: 2PNE 	<p><b>Organisms:</b> Primitive arthropod, Collembola <i>Hypogastrura harveyi</i> (snow flea) (Graham and Davies 2005).</p> <p><b>Structure:</b> Six antiparallel left-handed polyproline type II coils, tightly packed in two sets of three, making flat surfaces on both sides, one hydrophobic and one hydrophilic (Pentelute et al. 2008). Composed of GXY repeats. In the small isoform there are two S–S bonds, and one in the large isoform. Extremely thermolabile (Graham and Davies 2005). Size: <math>\sim</math>40 <math>\times</math> 10 <math>\times</math> 5 Å.</p> <p><b>Isoforms:</b> One small (6.5 kDa) and one large (15.7 kDa).</p> <p><b>IBS:</b> putatively the hydrophobic side of the flat disk.</p> <p><b>Planes bound:</b> Multiple, including the basal (Mok et al. 2010).</p> <p><b>Activity:</b> High TH (hyperactive). Produces rice grain-shaped crystals (Graham and Davies 2005; Mok et al. 2010).</p>
LpIBP  PDB: 3ult	<p><b>Organisms:</b> Plant: rye grass (<i>Lolium perenne</i>).</p> <p><b>Structure:</b> 12-kDa <math>\beta</math>-solenoid with 8 coils composed of tandem repeats of the 7-aa consensus sequence XXNXVXG, repeating twice in each coil. The first three coils contain one more residue per loop, which make a bulge on one side of the solenoid (Middleton et al. 2012). Size: <math>\sim</math>33 <math>\times</math> 20 <math>\times</math> 10 Å.</p> <p><b>Isoforms:</b> Several, most are linked to a N-terminal Leucine-rich repeat domain of unknown function. One contains an extra loop (Kumble et al. 2008).</p> <p><b>IBS:</b> A flat <math>\beta</math>-sheet with imperfect rank of TXT motifs (<math>\sim</math>30% Thr, most other residues are Ser, Ala, and Val) (Kumble et al. 2008).</p> <p><b>Planes bound:</b> Primary prism and basal planes (Middleton et al. 2012).</p> <p><b>Activity:</b> Low TH, high ice recrystallization inhibition. Produces flat-tipped, hexagonal-shaped ice crystals that grow in all directions once the freezing point is exceeded.</p>

(continued)

**Table 4.1** (continued)

Name and structure	Details
<p data-bbox="150 234 330 261"><i>TisAFP</i> and <i>LeAFP</i></p>  <p data-bbox="150 564 262 590">PDB:3UYU</p>	<p data-bbox="371 234 1024 340"><b>Organisms:</b> Microorganisms. Examples: snow mold fungus <i>Typhula ishikariensis</i> (<i>TisAFP</i>) (Kondo et al. 2012); Arctic yeast <i>Leucosporidium</i> sp. (<i>LeAFP</i>) (Lee et al. 2012). Many homologs in bacteria, fungi, algae, and diatoms.</p> <p data-bbox="371 342 1024 472"><b>Structure:</b> 23 kDa, right-hand <math>\beta</math>-solenoid with a triangular cross section composed of 6 coils with 18 (or more) aa per coil alongside an <math>\alpha</math>-helix. The sequence is non-repetitive with no consensus motif (Kondo et al. 2012). <i>LeAFP</i> has a glycosylated residue and a C-terminal loop that makes it a dimer (Lee et al. 2012). Size: <math>\sim 47 \times 30 \times 27</math> Å.</p> <p data-bbox="371 474 1024 525"><b>Isoforms:</b> Several isoforms with poorly conserved IBSs and range of activities from moderate to hyperactive.</p> <p data-bbox="371 527 1024 601"><b>IBS:</b> A flat but irregular face on the solenoid with no repeating motif and no conserved residues in homologs. Probed by mutagenesis in <i>TisAFP6</i> (Kondo et al. 2012)</p> <p data-bbox="371 603 1024 677"><b>Planes bound:</b> Various depending on isoform studied; e.g., basal plane and additional sixfold plane that is not primary or secondary prism for <i>TisAFP6</i> (Kondo et al. 2012).</p> <p data-bbox="371 679 1024 784"><b>Activity:</b> Produces crystal shapes that can be pitted bipyramids. Most variants have moderate TH and burst along the <i>c</i>-axis. At least one homolog (<i>TisAFP8</i> isoform) is hyperactive and bursts normal to the <i>c</i>-axis (Kondo et al. 2012).</p>
<p data-bbox="150 793 262 820"><i>MpIBP-RIV</i></p>  <p data-bbox="150 1111 256 1137">PDB:3P4G</p>	<p data-bbox="371 793 1024 844"><b>Organisms:</b> Antarctic bacterium: <i>Marinomonas primoryensis</i> (Garnham et al. 2011a).</p> <p data-bbox="371 846 1024 920"><b>Structure:</b> The ice-binding domain <i>MpIBP-RIV</i> of the bacterial adhesin is a 34 kDa, <math>\beta</math>-solenoid with 13 tandem repeats of 19-residue coils. <math>\text{Ca}^{2+}</math> ions inside the coils rigidify the IBS. Size: <math>\sim 70 \times 27 \times 17</math> Å.</p> <p data-bbox="371 922 597 949"><b>Isoforms:</b> None detected.</p> <p data-bbox="371 950 1024 1001"><b>IBS:</b> Two parallel rows of outward projecting residues, one Thr, the other Asx.</p> <p data-bbox="371 1003 742 1030"><b>Planes bound:</b> Multiple, including basal.</p> <p data-bbox="371 1031 1024 1106"><b>Activity:</b> The recombinant <i>MpIBP-RIV</i> is hyperactive but functions as a bacterial ice adhesin rather than an antifreeze (Bar Dolev et al. 2016a; Guo et al. 2012).</p>
<p data-bbox="150 1146 262 1173">Midge AFP</p>  <p data-bbox="150 1428 223 1455">(model)</p>	<p data-bbox="371 1146 867 1173"><b>Organisms:</b> Midge (<i>Chironomidae</i>) (Basu et al. 2016).</p> <p data-bbox="371 1174 1024 1280"><b>Structure:</b> Tight left-handed solenoid composed of 8 coils of 10-residue tandem repeats of CXGX<math>\text{Y}</math>CXGX. Eight disulfide bonds crosslink the coils. The solenoid is so tight that there is no <math>\beta</math>-strand character. Size: <math>\sim 40 \times 20 \times 15</math> Å.</p> <p data-bbox="371 1282 1024 1333"><b>Isoforms:</b> Four isoforms with minor sequence differences and variations in the number of coils.</p> <p data-bbox="371 1335 1024 1386"><b>IBS:</b> Predicted to be a row of Tyr stacked 4.5 Å apart on one face of the solenoid.</p> <p data-bbox="371 1388 1024 1439"><b>Planes bound:</b> Pyramidal plane intermediate between basal and prism planes. Produces bipyramidal ice crystals.</p> <p data-bbox="371 1441 930 1467"><b>Activity:</b> Intermediate TH activity. Burst normal to the <i>c</i>-axis.</p>

Color code: alpha-helix, red; beta-strands, yellow; coil, green; disulfide bonds, orange;  $\text{Ca}^{2+}$ , blue

AFPs and the bacterial ice adhesin from *Marinomonas primoryensis*. Many of the IBPs have multiple isoforms that vary in size and activity. In general, the larger the isoform, the higher is its TH activity. Although there is no crystal structure for the antifreeze glycoproteins (AFGPs), it is likely they fold as a polyproline type II helix because this will fit the three-residue periodicity (Table 4.1) and produce an amphipathic helix that seems so important to the functioning of type I AFP (Baardsnes et al. 1999; Graham et al. 2013). Fish type IV AFPs are not listed in the table because recent evidence suggests they do not function as IBPs in nature (Gauthier et al. 2008).

Some of the recently published IBP structures possess interesting characteristics that have led to new questions and a broadening of the scope of the structure–function relationship in IBPs. One example is the hyperactive IBP from winter flounder: Maxi. This protein forms a homodimer in solution, with no stable monomer form. The monomer of Maxi is like a fivefold longer version of the small type I AFP from the same fish. One wonders how this giant version of type I AFP evolved and whether it preceded or followed on from the small single helix (Sun et al. 2014). What is especially puzzling in this context is that the role of the ice-binding residues in type I AFP changes in Maxi into forming and maintaining the interior network of 400 clathrate waters that hold the four-helix bundle structure together. Another interesting example of structure–function relationships is the IBP from the Antarctic bacterium *Marinomonas primoryensis* (*MpIBP*). The molecular weight of *MpIBP* is >1.5 MDa, consisting of ~130 domains. The structure of this protein can be broken down into five regions, only one of which (*MpIBP*-RIV) binds ice. *MpIBP*-RIV is a single domain that folds into a  $\beta$ -solenoid with a row of  $\text{Ca}^{2+}$  ions stabilizing the helical structure (Garnham et al. 2011a). When this region was recombinantly expressed, it had the high TH values and ice-shaping characteristics of a hyperactive IBP (Garnham et al. 2008). However, *MpIBP* is an ice adhesin in its natural context (Bar Dolev et al. 2016a), and its other regions have other specific roles (Guo et al. 2012, 2017; Vance et al. 2014). This is an unusual function for an IBP (Bar Dolev et al. 2016a) but there is now evidence that the DUF3494 fold has been co-opted into this adhesion function in another marine bacterium (Vance et al. 2018).

### 4.3 Identification and Mapping of Ice-Binding Sites

Each IBP has a surface—the IBS—that has evolved to dock the protein to ice (Fig. 4.1). The key to experimentally defining this surface has been to produce the IBP as a recombinant protein (Chao et al. 1993), solve its 3-D structure (Sonnichsen et al. 1993), and then probe the extent of the IBS using site-directed mutagenesis (Chao et al. 1994). This process is nicely illustrated by studies on type III AFP, the first IBP for which the IBS was experimentally defined. Type III AFP is a good case in point because the IBS of this AFP could not be initially predicted by flatness and regularity as it had been for type I AFP (DeVries and Lin 1977) and subsequently was for AFPs like *TmAFP* (Liou et al. 2000) and *Rhagium inquisitor* AFP (*RiAFP*)



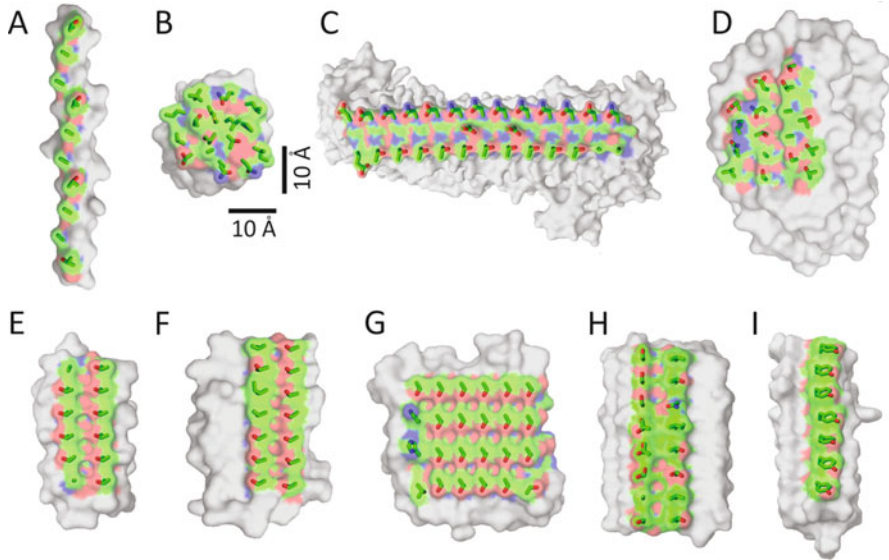


**Fig. 4.1** Ice-binding sites of IBPs. IBP structures are shown in surface presentation and are to scale. Residues of the experimentally determined or putative IBSS are colored (carbon atoms in green, oxygen in red, and nitrogen in blue). Non-IBS residues are in gray. Stick representation of the IBS residue side chains are overlaid on each structure. (a) Type I AFP from winter flounder. PDB 1WFA (Sicheri and Yang 1995). (b) Type III AFP from ocean pout, isoform HPLC12. PDB 1MSI (Jia et al. 1996). (c) Region IV of the ice adhesin from *Marinomonas primoryensis* (MpIBP-RIV). PDB 3P4G (Garnham et al. 2011a). (d) Snow mold fungus IBP from *Typhula ishikariensis*, moderately active isoform (*Tis*AFP6). PDB 3VN3 (Kondo et al. 2012). (e) *Tenebrio molitor* AFP (*Tm*AFP), isoform 4–9. PDB 1EZG (Liou et al. 2000). (f) Spruce budworm AFP (*sbw*AFP), isoform 501. PDB 1M8N (Leinala et al. 2002). (g) *Rhagium inquisitor* AFP (*Ri*AFP). PDB 4DT5 (Hakim et al. 2013). (h) *Lolium perenne* AFP (*Lp*AFP). PDB 3ULT (Middleton et al. 2012). (i) Model of midge AFP (Basu et al. 2015)

(Hakim et al. 2013). The only other indicator for IBS function in this initial study was the conservation of the residues that make up the IBS when aligned to a dozen different isoforms. Conserved internal residues are probably essential for the protein fold. But conserved surface residues, especially those that form a patch, are likely to be involved in the function of the protein, which in this case is ice binding. The conserved surface residues of type III AFP first targeted for mutagenesis included T18, N14, and Q44. The initial rationale for the mutagenesis choices, when it was still thought that IBPs bound to ice through a hydrogen-bonding network (DeVries and Lin 1977; Wen and Laursen 1992a), was to disturb this hydrogen-bonding pattern, as for example with the effective mutants T18N, N14S, and Q44T.

When it was realized that the IBS was the most hydrophobic surface of the IBP (Sonnichsen et al. 1996) and the hydrophobic effect was speculated to be the binding force for holding the IBP on ice, the success of these mutagenesis experiments was attributed to steric hindrance to binding when replacing a small side chain with a larger one (DeLuca et al. 1996), or to spoiling the “snug” fit when the replacement



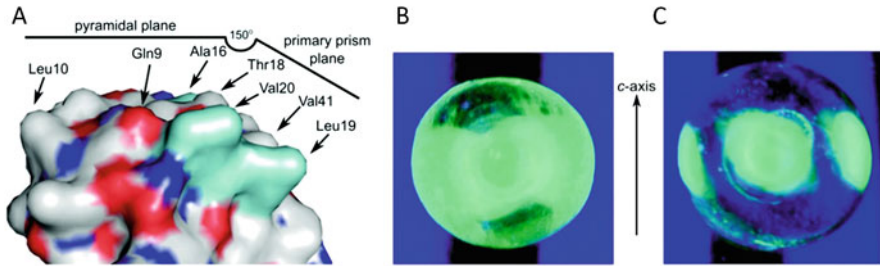


**Fig. 4.2** Compound ice-binding site of type III AFP from ocean pout (QAE1 isoform, also called HPLC12). (a) The ice-binding site of type III AFP showing its two adjacent subsites, each binding a different plane or set of planes of ice. (b–c) FIPA analysis of (b) a GFP-labeled wild-type protein and (c) a GFP-labeled A16H mutant. The single-crystal ice hemispheres were mounted with the secondary prism plane oriented normal to the long axis of the cold finger. The large fluorescence signal in **b** indicates binding to more than the primary prism plane of ice. The reduced fluorescence in **c** demonstrates that the mutant has reduced ice-plane activity. There is no binding on the top and bottom of the hemispheres because the proteins do not bind the basal plane of ice. Reprinted (adapted) with permission from (Garnham et al. 2010) Copyright (2010) American Chemical Society

was smaller than the original residue (Baardsnes and Davies 2002). In the latter study, a series of replacements of hydrophobic residues on the IBS of type III AFP with generally smaller side chains were detrimental to antifreeze activity as measured by thermal hysteresis (TH). Currently, the binding mechanism of IBPs to ice is thought to be due to the anchored clathrate water hypothesis (Garnham et al. 2011a) where the hydrophobic groups on the IBS are caged by water molecules that are linked and stabilized by hydrogen bonding to nearby hydrophilic groups (discussed in Sect. 4.10). In retrospect, changing the shape and hydrogen bonding capabilities of residues on the IBS would also interfere with ice binding by this anchored clathrate water mechanism.

Another complication added to the difficulty of defining the IBS of type III AFP is that the most active isoforms have two adjacent IBSs on an angle to each other. Together they form a compound IBS (Fig. 4.2) (Garnham et al. 2010). These QAE1 isoforms bind to both the primary prism and a pyramidal plane. However, the SP and QAE2 isoforms bind only to the pyramidal plane, and as such can slow the growth of ice but not stop it. These adjacent IBSs have been defined by site-directed mutagenesis, and have been validated by fluorescence-based ice plane affinity (FIPA) analysis. The proof of principle has come from an engineering study where an inactive QAE2 isoform was converted into a fully active form by as few as four surface mutations (Garnham et al. 2012).

What should have been a simpler study system for defining the IBS has been the type I AFP from righteye flounders (Sicheri and Yang 1995). This single  $\alpha$ -helix was initially predicted to bind ice by hydrogen bonding from the regularly spaced Thr and Asx residues (Chou 1992; Wen and Laursen 1992a). The periodicity of these Thr and Asx places them on the same side of the helix at 11 residues apart each. The 37-residue HPLC-6 isoform of type I AFP is small enough for production in a good

yield and at reasonable cost by solid-phase peptide synthesis. Thus, numerous variants were made to test the binding hypothesis. Replacement of the putative ice-binding Thr by Ser or Val proved to be informative (Chao et al. 1997; Haymet et al. 1998, 1999; Zhang and Laursen 1998). Change of the central two Thr to Ser caused a major loss of activity whereas the switch to Val had minimal effect (Chao et al. 1997). This emphasized the importance of the Thr methyl groups relative to the hydroxyls. Again, alignment of isoforms and orthologues was highly informative in defining the IBS to be conserved Thr and Ala residues on the same side of the helix. The role of the Ala residues was confirmed by the synthesis of steric substitutions where Leu replaced Ala. The role of Thr and adjacent Ala in ice binding fits well with the anchored clathrate water hypothesis. Waters around the methyl groups of these ice-binding residues can be anchored to the Thr OH group or to the peptide backbone that is accessible to solvent waters due to the high Ala content (65%) of the helix. Although this clathrate water pattern was not seen in the original X-ray crystal structure of winter flounder type I AFP because the protein was crystallized in acetone (Sicheri and Yang 1995), this clathrate arrangement has been recently seen in the crystal structure of Maxi, an extremely divergent isoform of type I AFP. Maxi can serve as a surrogate to show approximately what the anchored clathrate waters might look like on the ice-binding residues of type I AFP (Sun et al. 2014).

The identification and mapping of an IBS by site-directed mutagenesis has even worked well with models of an IBP before its structure was determined by crystallography or nuclear magnetic resonance (NMR). A convincing example of this method was the systematic mutagenesis of the ice-binding domain of the giant ice adhesin from the Antarctic bacterium *Marinomonas primoryensis*. Having modeled this domain as an extended beta-solenoid, a series of outward pointing steric mutations (and one inward pointing one) were made at intervals around the circumference of the solenoid. Mutations on the outer surface that curve around the inner row of  $\text{Ca}^{2+}$  ions severely attenuated TH activity, whereas those elsewhere on the surface had no significant effect. The internal mutation that tried to place an arginine side chain into the protein interior (V93R) was also highly detrimental. Thus the mutation study first validated the modeled protein fold by confirming the outward and inward pointing residues, and then revealed that the IBS was composed of the two parallel rows of Thr and Asx that run the length of the solenoid on one side (Garnham et al. 2008).

#### 4.4 Planes Bound by AFPs

One outcome of the structural diversity of IBPs is they can have different ice plane binding preferences. That their IBSs have different functional residues and different spacing between exposed chemical groups grants them specificity for particular planes of ice in specific orientations. When an IBP molecule sticks to its energetically favored site on ice, ice growth in the vicinity slows down. Because of the

periodicity of ice crystals, multiple IBP molecules of the same type bind to adjacent, equivalent sites on the ice plane. Consequently, a facet is developed. This binding specificity is remarkable because the IBP targets a specific pattern of crystalline water molecules among many similar possibilities in a situation where the ice is surrounded by a huge excess of liquid water in which IBPs are freely soluble. Also, the ice surface is not directly exposed to IBPs but is coated by a thin layer of quasi-liquid water (Hayward and Haymet 2001; Limmer 2016). The answer to how each IBP binds to a specific plane at the molecular level is still somewhat speculative. Ice-etching studies (see Chap. 9 of this volume for details on the method) conducted in the early 1990s have shown that type I AFPs, which are short repetitive peptides, from the winter flounder (*Pseudopleuronectes americanus*) and the closely related Alaskan plaice (*Pleuronectes quadritaberulatus*) bind to the  $[\bar{2} 0 2 1]$  pyramidal planes of ice. However, type I AFP (SS-8 isoform) from shorthorn sculpin (*Myoxocephalus scorpius*) adsorbs onto  $[2 \bar{1} \bar{1} 0]$ , the secondary prism planes (Knight et al. 1991). Although these two versions of type I AFP share high sequence identity, they are not homologues. They arose independently to form similar IBPs by a remarkable case of convergent evolution (Graham et al. 2013). Indeed, the fact that the flounder and sculpin type I AFPs bind to different planes of ice is an additional argument for their independent origins. Ice etching of two type III isoforms (AB1 isoform of *A. brachycephalus* and the HPLC12 isoform of *M. americanus*) revealed a more complex pattern, suggesting that both proteins bind to several ice planes including the primary prism plane  $[1 0 \bar{1} 0]$ , the pyramidal plane  $[2 0 \bar{2} 1]$ , and some additional planes inclined by a small rotation from these planes (Antson et al. 2001). Thus, an AFP that binds to several ice planes can still have moderate TH activity. The compound IBS of type III AFP which consists of two adjacent parts juxtaposed at an angle of  $150^\circ$  to each other (Fig. 4.2) clearly demonstrates how the protein binds to more than one crystallographic plane (Garnham et al. 2010).

A growing number of IBPs have been shown to bind the basal plane of ice. Most of these proteins have particularly high TH activities, for which they are termed “hyperactive.” In fact, the hyperactivity of IBPs has been linked to their ability to adhere to the basal plane of ice in addition to other planes, and stop ice growth along both the *a* and the *c* directions (Scotter et al. 2006; Pertaya et al. 2008). Ice etching studies of the *Choristoneura fumiferana* (spruce budworm) AFP (sbwAFP) showed that it binds to the primary-prism plane and the basal plane (Graether et al. 2000). The fluorescence-based version of the ice etching method, FIPA analysis (Basu et al. 2014), yielded an ice crystal covered from all directions when grown in *Tm*AFP (Basu et al. 2014) and *Ri*AFP (Hakim et al. 2013) solutions (Fig. 4.3e and g, respectively), as did a more potent isoform of sbwAFP, isoform 501 (Fig. 4.3f). This suggests that these proteins can bind to multiple planes of ice. The abovementioned three IBPs have repetitive structures with well-defined IBSs, determined from 3-D crystal structures, modeling, and, in the cases of *Tm*AFP, by extensive surface mutagenesis studies (Marshall et al. 2002). The IBSs of these proteins are flat and composed of multiple arrays of outward pointing threonine residues that presumably bind to several ice planes. This is in contrast to the IBS of

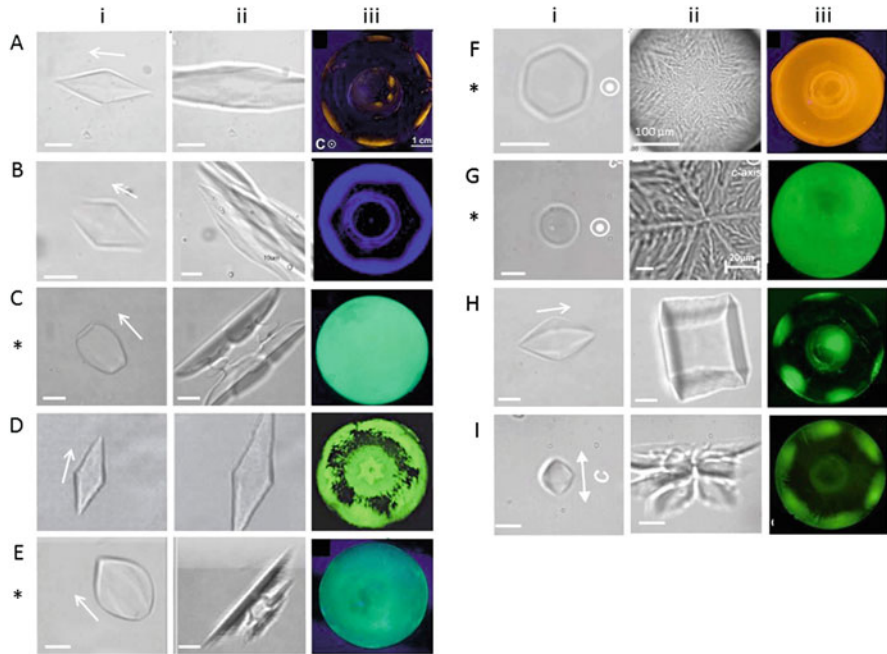


**Fig. 4.3** Comparison of ice-binding properties of IBPs. Typical morphology of IBP-bound ice (i) within the TH gap and (ii) just after the burst. The white arrow indicates the direction of the *c*-axis. (iii) FIPA analysis with the *c*-axis normal to the field of view. (a) Type I AFP from winter flounder (Bar Dolev et al. 2012; Basu et al. 2014). (b) Type III AFP from ocean pout, isoform HPLC12 (Bar Dolev et al. 2012; Basu et al. 2014). (c) *Mp*IBP-RIV (Bar Dolev et al. 2012; Basu et al. 2014). (d) Snow mold fungus IBP from *Typhula ishikariensis*, moderate isoform (*Tis*:AFP6) (Kondo et al. 2012; Xiao et al. 2010). (e) *Tm*AFP, isoform 4–9 (Bar et al. 2008a; Basu et al. 2014). (f) *sbw*AFP, isoform 501 (Bar Dolev et al. 2012; Basu et al. 2014). (g) *Ri*AFP (Hakim et al. 2013). (h) *Lp*AFP (Middleton et al. 2012). (i) Midge AFP (Basu et al. 2016). Images reprinted from the above references with permission. An asterisk on the left indicates that the IBP is hyperactive. Scale bars are 10  $\mu\text{m}$  unless otherwise specified

type III AFP, which binds different planes from distinct positions on its compound IBS (Garnham et al. 2010). Another interesting example is the IBP from ryegrass (*Lp*IBP), which binds to both the basal plane and the primary prism plane (Middleton et al. 2012), the same planes bound by *sbw*AFP. However, *sbw*AFP is hyperactive with a TH activity that exceeds 5 °C at 1 mg/ml concentration (for the 501 isoform). On the contrary, *Lp*AFP has low TH activity, in the range of 0.3 °C at a concentration of 2 mg/ml. The two proteins are approximately of same size (~12 kDa), but the ice-binding site of *Lp*IBP is less repetitive than that of *sbw*AFP, and the ice hemisphere grown in *Lp*IBP solution (Fig. 4.3h) is less covered by protein compared to the hemispheres grown with the insect proteins (Fig. 4.3e–g). The recently characterized IBP from midge binds to a pyramidal-ice plane positioned intermediate between the basal and primary prism planes. This plane is different from those observed with other moderate IBPs, and it seems to be at least partially responsible

for the intermediate TH activity of this protein, higher than the moderately active IBPs, but lower than that of the hyperactive proteins (Basu et al. 2016). Another example of unusual ice binding is EfcIBP (a DUF3494-type protein) that shows basal plane affinity without prism plane affinity and has moderate TH activity (Kaleda et al. 2019; Mangiagalli et al. 2018). This points to the possibility of a broader spectrum of yet undefined IBPs that have activities between moderate and hyperactive.

## 4.5 Ice Shaping

The fundamental ability of IBPs to bind to ice can cause outward growth of the bound surface to cease as dictated by the Gibbs–Thomson effect (Wilson 1993). This growth inhibition leads to the formation of ice shapes distinct from the disk shape of ice in pure water (Kawahara 2013). Examples of shapes induced by IBPs are shown in Fig. 4.3(i). The same effect causes inhibition of melting, which also leads to ice shaping (Bar Dolev et al. 2012; Liu et al. 2012; Pertaya et al. 2007a). The specificity of IBPs for different ice planes and the ice-binding rates of each protein to each ice plane dictate the particular ice shapes, characteristic of an IBP type. We describe ice shaping in the presence of IBPs in three separate temperature regimes: below the hysteresis freezing point (the “burst” pattern), above the hysteresis freezing point (within the TH gap), and above the melting point (melting pattern).

### 4.5.1 Ice Shaping Below the Hysteresis Freezing Point

When a supercooled ice crystal is brought to its freezing point, sudden fast growth is observed. This “burst” temperature defines the freezing point of the crystal and the lower limit of the TH gap. Proteins with high TH values, such as the hyperactive insect IBPs, can supercool for several degrees, so the burst is abrupt with a dendritic growth pattern (Fig. 4.3(ii), c, e–g). Proteins with low TH can produce milder burst forms, including just a steady increase in the size of the crystal in all dimensions, an example of which is provided by the plant IBP, *LpAFP*. The direction to which the crystal grows during the burst is dependent of the IBP-covered planes. In general, IBPs that can bind the basal planes will direct the ice burst normal to the *c*-axis, while IBPs that do not bind the basal plane induce the ice burst along the *c*-axis (Scotter et al. 2006). Still, there are differences in the burst pattern among the non-basal binding IBPs. For example, in type I and type II fish AFPs solutions the ice bursts as a single sharp needle emerging from the tip of the crystals, while in type III AFP solutions many small crystals emerge from the original one at the burst (Fig. 4.3(ii), a–b). An interesting case is *LpAFP*, which binds to both basal and prism planes and has low TH activity (Middleton et al. 2012). This leads to the growth of ice shaped like a hexagonal box (Bar Dolev et al. 2012; Middleton et al. 2012) (Fig. 4.3(ii), h).

The recently characterized midge IBP is an example of a protein that does not bind the ice basal plane and yet causes the ice crystal to burst perpendicular to the  $c$ -axis (Fig. 4.3(ii), i) (Basu et al. 2016). Another interesting example is type I AFP from a righteye flounder, the barfin plaice (bpAFP), that has exceptionally high solubility (Mahatabuddin et al. 2017). At low concentrations, bpAFP behaves as a typical type I AFP with pyramidal plane binding, low TH activity, and directs crystal burst along the  $c$ -axis. At high concentrations, TH values can reach 3 °C and the ice crystal bursts perpendicular to the  $c$ -axis. In this regard, bpAFP behaves more like Maxi, and there is indeed evidence for oligomerization. Recently, a Saturn-like shape has been observed as the burst growth pattern of ice in efcIBP solution. This growth pattern is consistent with the affinity of efcIBP for the basal plane of ice without affinity for the prism plane (Kaleda et al. 2019).

### 4.5.2 Ice Shaping Within the TH Gap

The bipyramidal ice shapes in solutions of moderate fish AFPs are widely documented (Bar Dolev et al. 2012). However, a careful examination showed that below and close to the melting point, the crystals have the form of truncated bipyramid, with some exposed basal plane. At lower temperatures, the crystals continue to grow in the  $c$  direction, and the basal planes shrink until they reach a critical size on which new layers of water cannot be incorporated (Knight and DeVries 2009). At this stage, the crystal is populated by IBP molecules on all 12 equivalent surfaces of the hexagonal bipyramid, which is the basis for their ability to arrest ice growth. At lower temperatures, the critical size for ice nucleation is smaller, so the tips continue to grow and become sharper. These tips are protected less effectively relative to the crystal planes and the burst usually starts from them. In the case of the hyperactive IBPs, which bind to the basal planes, the ice crystals are covered by proteins from all directions (Pertaya et al. 2008), so they are protected from growth (and melting) throughout the TH gap. Therefore, the growth of pyramidal tips is not apparent, and their shapes remain constant (Bar Dolev et al. 2012).

In the early 1990s, researchers noted that at varying low concentrations of type I AFP from winter flounder ice crystals always grew with a constant  $c:a$  axis ratio of 3.3:1. This ratio remained constant also in a series of mutants with lower TH activities relative to the wild type. However, the axis ratio of ice crystals in dilute solutions of type III AFP from ocean pout (QAE1 isoform) changed as the crystal continued to grow and changed with AFP concentration. In addition, partially inactivated type III AFP mutants produced different axis ratios (DeLuca et al. 1996). A theory developed to explain this phenomenon suggests that the flounder AFP, which binds only to one pyramidal plane of ice, is aligned on the pyramidal planes without forming steps. Type III AFP binds to prismatic planes, so it was reasoned that steps must form in order to get pyramidal shapes. The length of each step is concentration dependent, which leads to variation in the axis ratio at different protein concentrations (DeLuca et al. 1996). However, another type I AFP from



sculpin adsorbs on the secondary prism planes (Knight et al. 1991), which seem to require a step-growth mechanism to achieve a bipyramidal ice crystal shape. Later studies showed that type III binds to more than the prismatic plane (Antson et al. 2001; Garnham et al. 2010) adding complexity to this phenomenon. A plausible scenario to explain the changes in axis ratios due to concentration or mutagenesis is that ice growth velocities depend on the adsorption rates of each protein to a particular ice plane (Drori et al. 2014a; Knight and DeVries 2009).

### 4.5.3 *Ice Shaping at Melting*

Bipyramidal ice crystals in moderate IBP solutions always start to melt from their tips, where ice coverage is less effective. The melting advances along the *c*-axis, exposing more basal surface until the crystal obtains an eye shape with tips normal to the *c*-axis (Bar Dolev et al. 2012). Hyperactive IBPs, which effectively bind the basal planes, result in characteristic ice shaping during melting (see Fig. 4.3(i)—c, e, f, and g). This is counterintuitive because the crystal is retreating. However, it was shown that IBPs can slow down ice melting, and even completely inhibit melting, resulting in superheated ice (Celik et al. 2010; Cziko et al. 2014; Knight and DeVries 1989). Furthermore, the methods used to observe crystal shaping include flash freezing of the whole solution, so the melting shapes are possibly formed due to protein trapped in the crystal. The variations in the shapes obtained with each IBP during melting are related to differences in the melting velocities on the *a* and the *c* axial directions. A model of ice melting that considers low melting velocity in the *c* direction relative to the *a* direction successfully predicted the formation of the lemon shape structure, characteristic of *TmAFP* (Liu et al. 2012).

## 4.6 Size and Cooperative Effects of IBP Activity

### 4.6.1 *Size of AFP Molecule and Cooperativity*

One puzzle in understanding IBP activity was the observation that TH appears only above a certain protein concentration threshold. Below this concentration, AFPs were sufficient to shape ice but not arrest its growth. An early model proposed that at high protein concentrations there is a cooperative effect: protein molecules form side-by-side interactions that create an AFP patch with several IBS aligned on the ice surface (Wen and Laursen 1992a). To test this hypothesis, the 7-kDa type III AFP was fused to 12-kDa or 42-kDa proteins, increasing its overall size to ~20 and ~50 kDa, respectively. It was expected that the TH activity of the fusion protein would be lower than the TH of the wild type because the fused proteins impose a steric intervention and disrupt any possible side-by-side AFP interactions. However, the opposite was observed. Larger (bulkier) conjugates resulted in greater TH

activity (DeLuca et al. 1998). These findings rule out the hypothesis of the cooperative binding effect of AFP patches and they are supported by the adsorption–inhibition model (Raymond and DeVries 1977) and the Kelvin effect (Wilson 1993). Increasing the size of AFPs reduces the distance between adjacent molecules since each molecule covers more of the ice surface. This lowers the probability of water addition on the ice surface and lowers the freezing point. We have tested green-fluorescent protein (GFP) fusions of AFP type III and the hyperactive *TmAFP* (9 kDa), where the GFP molecule (26 kDa) increases the overall size of the proteins ~fourfold. We observed that GFP fusions are >twofold more active than unconjugated *TmAFP* on a molar basis. Another study demonstrated that addition of low concentrations of polyclonal antibodies raised against *TmAFP* or its homolog from the beetle *Dendroides canadensis* (*DcAFP*) to the antigen solution enhanced the TH activity severalfold. The addition of secondary antibodies (goat anti-rabbit) that bound to the primary antibodies raised the TH even more (Wu et al. 1991). Clearly, larger IBPs lead to higher TH levels. These observations raise the question, why did IBPs evolve to be small, highly expressed proteins? Low-level expression of bigger proteins might have been metabolically favored. It may be that smaller molecules have increased accessibility to other areas in the body through extravasation from the circulatory system (Bar Dolev et al. 2016b). In addition, small molecules diffuse faster than larger ones. Notably, although side-by-side interactions between IBP molecules can be ruled out in the abovementioned examples, cooperative effects are still possible in certain cases. In a study of AFP type III from Notched-fin eelpout (*nfeAFP*), a significant increase in the TH activity of a barely active isoform was observed upon addition of low concentrations of a more active isoform. This may be due to a form of cooperativity between the two isoforms (Nishimiya et al. 2005; Takamichi et al. 2009) that likely involves the stabilization of binding planes for the less active isoform (Berger et al. 2019). In many fish and insects, low-active AFP isoforms have been identified in addition to moderate and hyperactive ones (Hew et al. 1988; Liou et al. 1999). Multiple isoforms may cooperate to provide better overall protection from ice growth.

#### 4.6.2 Size of IBS

The intuitive concept that IBPs with bigger IBSs will have higher antifreeze activities is consistent with both the reversible and irreversible ice-binding models (discussed in Sect. 4.11). IBPs with a larger IBS have a better chance to bind ice than those with a small IBS. It is also consistent with the hydration shell/anchored clathrate hypothesis (see Sect. 4.10), since a large IBS has more positions for binding water, which increases the likelihood of formation of a quorum of ice-like water molecules. This eventually increases the possibility of the clathrate waters on the IBP merging into the quasi-liquid layer at the ice–water interface and turning into ice. The advantage of a large IBS has been observed in organisms producing IBP

isoforms with different IBS sizes from either repetitive or non-repetitive structures, moderate and hyperactive.

Correlations between IBP size and TH activity are described in Chap. 3 of this volume. Here we specifically look at this relationship in isoforms of the same type where the structure of the IBSs is the same, but their sizes are different. One straightforward example is AFGPs. The small isoforms of AFGPs are much less potent than the larger ones, both natural (Wu et al. 2001) and synthetic (Tachibana et al. 2004), as shown in Fig. 3.1. Another example is the abundant 3.3 kDa  $\alpha$ -helical type I AFPs of the winter flounder, which consist of 3 repeats of the 11 amino acid (aa) consensus sequence. One isoform of this protein (AFP9) has 4 repeats of the consensus sequence and, therefore, a larger IBS surface area. This isoform had almost double the TH activity of the 3-repeat protein, although its size is only ~30% larger (Chao et al. 1996). Consistent with this size-to-activity relationship, a synthetic peptide consisting of only one repeating unit from the same AFP did not show any TH activity. The peptide did, however, produced ice shaping, indicating that it was still able to bind ice.

Two well-characterized isoforms of the hyperactive, left-handed  $\beta$ -helical AFP from spruce budworm (sbwAFP) are the 9 kDa (isoform-337) (Graether et al. 2000) and the 12 kDa (isoform 501), consisting of 5 and 7 helical loops, respectively. Parallel TXT motifs comprise the ice-binding face of both isoforms, but in isoform 501 there are two positions where Thr are replaced: in one case by Ile, and Val in the other. Although the overall IBS is only ~30% larger in isoform 501, its TH is three- to fourfold higher than that of the smaller isoform (Leinala et al. 2002), as shown in Fig. 3.7. In snow fleas, the TH of a larger isoform (15.7 kDa) is double the TH activity of a smaller isoform (6.5 kDa) at low concentrations (<0.2 mg/ml) (Graham and Davies 2005).

The Antarctic eelpout, *Lycodichthys dearborni*, produces a large type III AFP isoform called RD3 that consists of two consecutive units of the 7-kDa protein. The monomers are similar to each other in structure (Miura et al. 2001) and activity (Wang et al. 1995), and they are connected by a flexible 9-amino-acid linker. NMR studies indicated that this linker allows the simultaneous binding ice of both IBSs (Holland et al. 2008). A comparison of the TH activity of this tandem relative to the monomer is presented in Chap. 3 (Fig. 3.4). At low concentrations (<0.5 mM), the TH of the dimer reaches sixfold the activity of the monomers on a molar basis, although the overall size increased only twofold. Cooperative effects of the two units explained this significant enhancement (Miura et al. 2001; Wang et al. 1995). Notably, in this case both the size of the IBP and the size/number of the IBS were doubled. In a study of a recombinant model based on the RD3 dimer, where mutagenesis was used to knock out one of the IBSs, the IBS area contributed 80% of the increased TH activity, and the larger size accounted for the remaining 20% (Baardsnes et al. 2003). Previous studies with type III AFP fusion proteins had shown that TH activity increases with the overall size of the complex. A 20% increase in activity on doubling protein size was consistent with the range of increases seen with other naturally occurring isoforms (Chao et al. 1996; Leinala et al. 2002) and fusion proteins.

## 4.7 Protein Engineering of Better IBPs

IBPs have evolved on many occasions in different organisms to serve specific functions (Davies 2014). Those that serve as AFPs to prevent fish from freezing in icy seawater have a defined lower limit of  $\sim 1.2$  °C freezing point depression to achieve. This they accomplish with little leeway (Scotter et al. 2006), and only by producing high concentrations (mM) of AFPs in their blood. In several fishes these 10–30 mg/ml concentrations have required massive amplification of the AFPs genes to meet the concentration demand (Chen et al. 1997; Hew et al. 1988; Hsiao et al. 1990; Scott et al. 1988). Some terrestrial insects must overwinter at temperatures of  $-30$  °C without freezing. Based on in vitro assays of their AFPs it is likely that other factors besides TH contribute to this freezing point depression. Nevertheless, insect AFPs are considerably more potent at TH than fish AFPs. We attribute this hyperactivity to the ability of insect AFPs to bind the basal plane of ice in addition to other planes, as discussed in Sect. 4.4. Although there are hyperactive isoforms known for type I AFP, in general fish AFPs appear to be underachievers by not evolving basal plane binding. Why has evolution not made fish AFPs of greater potency, in lesser amounts, at a reduced metabolic cost? Although nature has not worked this way, hyperactive AFPs transgenically introduced into fish could potentially provide a biotechnological solution to the aquaculture of salmon in seawater areas where superchill mortality is a problem (Hew et al. 1992).

Aside from the lesson of basal plane binding, nature has provided other hints about how to improve on antifreeze activity. When there are multiple isoforms of a repetitive AFP, the bigger isoforms are invariably better at TH when compared on a molar basis (see discussion above, Sect. 4.6.2). This principle was confirmed in a protein engineering study where coils were added and subtracted from the  $\beta$ -solenoid structure of *Tm*AFP. Removal of just one coil from the seven found in the most abundant *Tm*AFP isoform caused a huge loss in activity; whereas the insertion of one or two coils had the opposite effect (Marshall et al. 2004a). How can this be rationalized when binding of an IBP to ice is necessarily irreversible? We can cite similar arguments used to explain why TH is a function of AFP concentration. Stopping a seed ice crystal from growing at supercooling temperatures requires diffusion and surface binding of sufficient AFPs to harness the Gibbs–Thompson effect. But for a productive contact that leads to binding between the IBP and ice, there must be a good match between the “anchored” clathrate waters on the IBS and the quasi-liquid water layer coating the ice surface. Having a larger IBS makes it statistically more likely that a match will be found.

Artificial constructs that multimerize IBPs have produced significant increases in antifreeze activity (Can and Holland 2011). These increases are optimally presented by the lower concentrations needed to achieve the same TH as free IBPs. The attachment of type I and type III AFPs to scaffolds like dendrimers demonstrates the potential of multimerization as a protein engineering approach to antifreeze enhancement, but it suffers from incomplete reaction (Stevens et al. 2015). A more controlled approach has been achieved through the use of self-assembling protein

cages (King et al. 2014; Padilla et al. 2001) to attach a fixed number of IBPs in a defined orientation with their IBSs projecting outward (Phippen et al. 2016). When TH activity is compared on a molar basis, a multimer displaying 12 IBPs is an order of magnitude more active than the monomer. This increase in freezing point depression is mirrored by a similar increase in the ability of the multimers to inhibit ice recrystallization. Following this approach there are many possibilities to form 1- 2- and 3-D arrays of different IBPs types and mixtures thereof to design ways to control and shape ice growth. Further details on this subject are given in Chap. 14 of this volume.

## 4.8 INPs: Ice-Nucleating Proteins

Ice-nucleating agents are widely dispersed in nature and serve to raise the temperature at which ice freezes by organizing an ice nucleus of sufficient size to promote its rapid growth (Pummer et al. 2015). Of relevance to this chapter are the biological ice-nucleating agents found on the surface of some bacteria. These INPs cluster together as aggregates on the bacterial surface that can promote freezing at temperatures as high as  $-2^{\circ}\text{C}$  (Guriansherman and Lindow 1993; Kawahara 2002; Kieft 1988; Wolber and Warren 1989). The primary sequence of these  $>120$  kDa bacterial INPs is composed of three regions. The central region is the largest and is a series of tandem 16-amino-acid repeats of consensus sequence GYGSTxTAxxxSxLxA, which promote nucleation (Green et al. 1988) (Warren and Corotto 1989). This repetitive region is flanked by shorter non-repetitive regions, the N-terminal one of which is thought to anchor the INP to the outer membrane of the bacterium (Kawahara 2002; Wolber and Warren 1989). Although there are no experimentally solved structures of INPs, some structural models for the repetitive region have been predicted (Guriansherman and Lindow 1993). Inspired by the  $\beta$ -helical folds of some insect AFPs (Graether et al. 2000; Liou et al. 2000), the repetitive regions of INPs from *P. syringae* (*Ps*INP) (Graether and Jia 2001) and a close relative *P. borealis*, (*Pb*INP) (Garnham et al. 2011b) were modeled as  $\beta$ -solenoids. The logic of this choice is that both IBPs and INPs have repeats of a similar length and that a solenoid fold places repeating motifs in line on the same face of the helix. In IBPs, the solenoid fold aligns the TXT ice-binding motifs into a two-dimensional array that functions as the IBS. As described in Sect. 4.10 below, the anchored clathrate water hypothesis for ice binding suggests that the IBS functions by organizing waters into an ice-like pattern sufficient to merge with the quasi-liquid waters on ice and in turn become ice. The fact that a solenoid fold for INP can potentially form an even longer array of TXT motifs strongly suggests a similar mechanism of surface water ordering. This hypothesis is strengthened by simulations of water molecules around the TXT arrays of the *Pb*INP model, showing that the INP could order water on this site (Garnham et al. 2011b). In INPs, the exaggerated length of the water-organizing region goes far beyond the six to eight coils needed for ice binding to a length where the excess ordered water can promote ice nucleation. Models have predicted a total

water-organizing area of  $4200 \text{ \AA}^2$  in *PsINP* (for a monomer) (Graether and Jia 2001), and  $25,600 \text{ \AA}^2$  in *PbINP* (for a dimer) (Garnham et al. 2011b). Taking into account that one INP molecule is necessary to obtain an ice nucleus at  $-12 \text{ }^\circ\text{C}$  (Govindarajan and Lindow 1988), the overall size of the water-organizing area of the INP models is roughly in agreement with the necessary size of ice nuclei at this temperature, which is  $20,100 \text{ \AA}^2$ . This calculation, together with several studies that showed INPs aggregate to facilitate nucleation at elevated temperatures ( $\sim -2 \text{ }^\circ\text{C}$ ) (Guriansherman and Lindow 1993), support the idea that INPs form ice by the same anchored clathrate water mechanism used by AFPs to bind ice (Garnham et al. 2011a). Thus, the basic difference between AFPs and INPs is their size. The large IBS of INPs can bind enough water molecules in an ice-like organization, sufficient to serve as a heterogeneous ice nucleus rather than suppress ice growth. Accordingly, some IBPs have slight ice nucleation activity, such as type I AFP at high concentrations (Wilson et al. 2010). Recent studies show low ice nucleation activity for type III AFP, *TmAFP*, and *sfAFP* that match the proteins' small size (Bissoyi et al. 2019; Eickhoff et al. 2019). Computational studies supported these findings (Qiu et al. 2019). Another study showed truncated INP has antifreeze activity (Kobashigawa et al. 2005). These results provide further support that INPs and AFPs bind ice by the same mechanism. On an issue of semantics, we include INPs in the group of IBPs not just because of their predicted common mechanism but because at the instant that INPs form ice they are effectively bound to its surface.

## 4.9 The Molecular Basis to Protein–Ice Interactions

The mechanism by which IBPs bind to ice at the molecular level has been an intensely debated topic in IBP research. The interface between protein and ice in an aqueous medium is difficult to probe experimentally and theoretically. Ice in water does not have clear boundaries between the crystalline and liquid states that can define a binding site at the molecular level. Instead, there is a thin zone (quasi-liquid layer) of water that is intermediate in state between solid and liquid water and effectively blurs the boundary between the two states (Hayward and Haymet 2001; Limmer 2016). Moreover, it is fascinating that IBPs can actually select particular ice surfaces, made up of only ordered water molecules, when they are surrounded by  $<55 \text{ M}$  of bulk water. Adding to these challenges is determining the IBS of many IBPs where there are no obvious motifs to help identify it and suggest a match to the ice. Even in the cases where the IBS are flat repetitive surfaces like *TmAFP* (Liou et al. 2000) and *RiAFP* (Hakim et al. 2013), there are numerous different ice planes that can be developed during growth when inhibitors such as IBPs are present. The differences between many of these planes (energetically or sterically) may be small enough to be practically indistinguishable.

Since the early studies of IBP mechanisms, many theories to explain the molecular basis for ice recognition by IBPs have been suggested (reviewed in (Davies et al. 2002; Vrielink et al. 2016; Yeh and Feeney 1996)). An early explanation was that the



abundant hydrophilic moieties on AFGPs immobilize water molecules in their vicinity and reduce the amount of water available for ice formation. This idea was disputed by NMR studies showing the amount of bound water molecules on AFGP surfaces is small (DeVries and Price 1984). It was then suggested that AFPs bind to ice through hydrogen bonds between protein side chains (or disaccharide moieties in the case of AFGPs) and available water molecules on the ice surface (DeVries and Price 1984; Knight et al. 1991). The low number of hydrogen bonds and their weakness in comparison to covalent bonds seemed insufficient to account for irreversible binding of IBPs to ice. An expansion of this idea based on an excellent match between the IBS and the bound ice plane was that hydroxyl groups on the protein surface could be incorporated into the ice lattice (Knight et al. 1993). However, mutagenesis studies of the IBS of type I AFP (Chao et al. 1997; Haymet et al. 1998; Zhang and Laursen 1998) and *Tm*AFP (Bar et al. 2008b) showed that the hydrophobic moieties on the IBS are more important than the surface hydroxyls for maintaining TH activity. Also, theoretical works showed that there is no gain of hydrogen bonds upon binding of type I AFP to ice (Madura et al. 2000; Wierzbicki et al. 2007).

## 4.10 The Hydration Shell Theory

Molecular dynamic simulations proposed that the first hydration layer on the IBS of type I (Yang and Sharp 2005) and type III (Smolin and Daggett 2008; Yang and Sharp 2004) AFPs makes a considerable contribution to the binding of the proteins to ice. These studies showed that apolar grooves in the IBSs of the proteins are filled with water molecules that are hydrogen-bonded to the polar groups on the IBS. These water molecules are arranged in a tetrahedral organization, similar to the organization of water molecules in ice. The quasi-ice layer bound to the protein facilitates merging of the protein to the quasi-liquid layer on ice in aqueous media (Gallagher and Sharp 2003; Wierzbicki et al. 2007). One experimental verification of this concept came from the crystal structure of ocean pout type III AFP, which was determined by combined X-ray and neutron diffraction data. Four water molecules arranged in an ice-like pattern were noted in the combined structure, suggesting that they were anchored in this organization to the protein in solution. However, only three of these water molecules were sufficiently well ordered to locate the hydrogen atoms in the crystal structure. The fourth water molecule in this water quorum was solved with partial occupancy (Fig. 4.4) (Howard et al. 2011).

Clearer evidence for ice-like water organization came from the crystal structure of the ice-binding domain of *Mp*IBP (*Mp*IBP-RIV). An array of ~50 water molecules arranged in an ice-like structure was present on the IBS of this protein (Fig. 4.5) (Garnham et al. 2011a). These waters formed cages around the surface methyl groups and this clathrate array was “anchored” to nearby hydroxyl and peptide backbone amide groups. Although ice-like ranks of water molecules were noted before in crystal structures of other IBPs (Liou et al. 2000), their IBSs were always

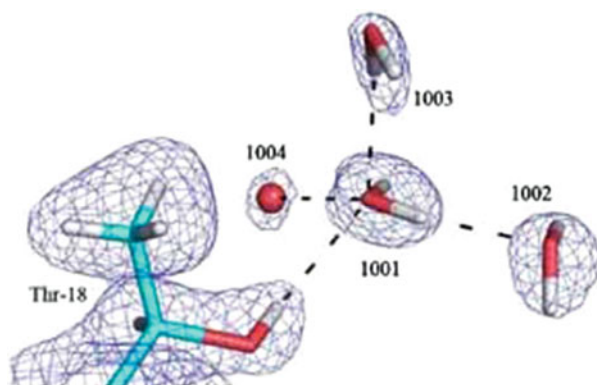


**Fig. 4.4** Ordered surface waters on the IBS of type III AFP. The tetrahedral water cluster model is superimposed on the  $\sigma_A$ -weighted  $2F_o - F_c$  nuclear scattering density map (contour level = 1 r.m.s.) for the tetrahedral water cluster. Note that while there are large nuclear scattering peaks for the three water molecules 1001, 1002, and 1003, the nuclear scattering peak for water 1004 is much weaker, indicating disorder. As such, it can only be modeled as an oxygen atom. Reprinted from (Howard et al. 2011). Copyright (2011) WILEY

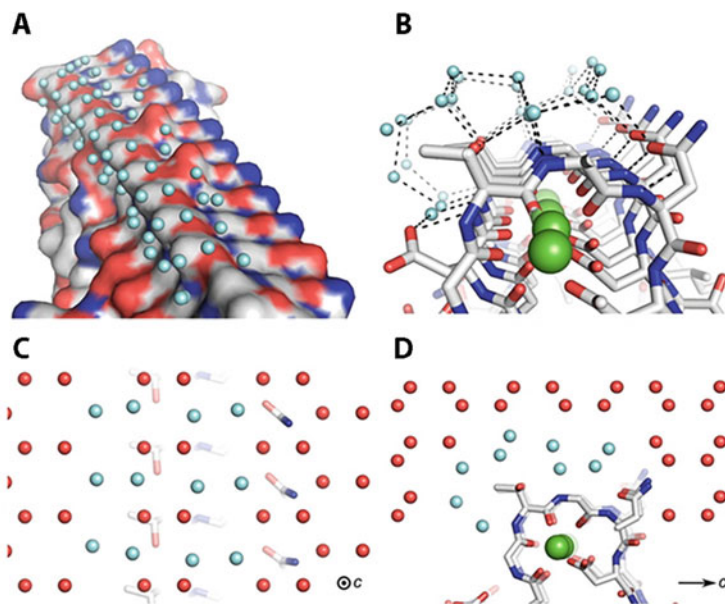


**Fig. 4.5** Ordered surface waters on the IBS of *MpAFP-RIV*. (a) Surface representation of the IBS of one of the protein molecules freely exposed to solvent in the unit cell. Carbon atoms are white, nitrogen are blue, and oxygen are red. Ordered surface waters are represented as aqua spheres. (b) Ordered surface waters showing some hydrogen bonded directly to the IBS. Structural  $\text{Ca}^{2+}$  ions are in green. (c–d) The organized surface waters make an excellent 3-D match to both the basal (c) and primary prism (d) planes of ice. The direction of the *c*-axis is indicated in both figures. Modified from (Garnham et al. 2011a)

directly opposed to the IBS of another IBP molecule, so the organization of any remaining water could be interpreted as a crystal-induced artifact. In the structure of *Mp*IBP-RIV, two out of the four protein molecules in the unit cell had their IBS exposed or partially exposed to the solvent, suggesting that the organization of surface waters was that seen in solution (Garnham et al. 2011a). Further support for the anchored clathrate water model has come from molecular dynamics (MD) simulations that showed ordered water structures on the IBS of *Tm*AFP (Yang et al. 2003) (Liu et al. 2016), sbwAFP (Nutt and Smith 2008), and *Pb*INP (Garnham et al. 2011b) in solution. While other simulations find only slight prestructuring of water molecules on the *Tm*AFP ice-binding surface in solution, they also support the formation of ordered water prior to the binding of AFP to ice, suggesting the need for ice to stabilize the clathrate water on the IBP surface (Hudait et al. 2018). In another experimental study, additional IBS-bound waters on type III AFP were revealed by crystallizing the protein as a fusion to maltose-binding protein that changes the orientation of the IBS toward the solvent (Sun et al. 2015). On a less active variant of the same AFP, mutations that improved activity were associated with a network of poly-pentagonal waters on the ice-binding face (Mahatabuddin et al. 2018).

An extension of the hydration shell theory suggests a contribution of the non-ice-binding faces of IBPs to their activity. MD simulations of the hydration shell around the three faces of the  $\beta$ -helical sbwAFP showed that while the ice-binding face facilitates the ordering of tetrahedral water structures, the other two faces disrupt water clusters such that ice-like water are excluded from those planes. It was concluded that the non-ice-binding faces of IBPs cooperate with the IBS by preventing overgrowth of the protein by the ice (Knight and Wierzbicki 2001; Nutt and Smith 2008).

Although the role of water molecules in the molecular recognition of ice by AFPs is thought to be generic to all IBPs, some controversies need to be resolved. Vibrational sum-frequency generation spectroscopy, which is similar to Raman scattering but sensitive only to molecules in nonsymmetric environments such as surfaces was used to observe the surface water molecules on the IBS of some IBPs. A clear peak attributed to the ice-like waters bound to the protein IBS in solution was present in the spectra of eelpout type III AFP but was absent in the spectra of an inactive mutant of the same protein. This peak was noted also in the spectrum of the wild-type protein taken at room temperature, although with lower intensity relative to that seen at low temperatures, indicating the stability of the ice-like water structure is dependent on temperatures (Meister et al. 2014). However, similar experiments with the hyperactive *Dc*AFP from beetles showed no such water organization. The authors concluded that the highly ordered  $\beta$ -helical *Dc*AFP does not need a water clathrate for ice recognition (Meister et al. 2015). Further contradictory data on *Tm*AFP, a homolog of *Dc*AFP, suggested the presence (Yang et al. 2003) or lack of (Modig et al. 2010) ice-like water molecules on its IBS. Another unresolved issue concerns the range of water molecules involved in ice recognition. An MD simulation on ocean pout type III AFP predicted that the water clathrate around the IBS of the protein consists of water molecules of the primary hydration layer but not beyond

(Smolin and Daggett 2008). However, terahertz absorption spectroscopy conducted to probe the long-range interactions of AFGPs (Ebbinghaus et al. 2010), type I AFPs (Ebbinghaus et al. 2012), and the hyperactive insect *DcAFP* (Meister et al. 2013) with water suggest that IBPs can retard hydrogen bond dynamics up to 20 Å from the protein surface. Although in the case of type I AFP a weakly active mutant had the same effect on the solution as the highly active wild-type protein (Ebbinghaus et al. 2012), the authors concluded that the long-range perturbation of solution dynamics is essential for ice recognition by IBPs. In a theoretical study of the first and second hydration shells of type III AFP it was found that the wild-type protein and two mutants with 10% and 54% of the wild-type activity had the same hydration properties. In this case it was suggested that there is no correlation between the effects of the proteins on the solvation water and the antifreeze activity (Grabowska et al. 2016). Clearly, the discrepancies between the abovementioned studies need to be resolved.

## 4.11 The Reversible–Irreversible Binding Conflict

The adsorption–inhibition theory (Raymond and DeVries 1977) suggests that IBPs bind to the surface of an ice crystal and pin it such that the ice can grow only between the bound protein molecules. This local pinning results in surface curvature that increases as the ice grows, leading to reduction of the freezing point due to the Gibbs–Thomson effect, and subsequently to inhibition of ice growth. The observation that ice growth can be completely stopped under supercooled conditions (in the TH interval) indicates that the IBPs bind irreversibly to the ice surface. If binding was reversible, ice would have grown at any position where an IBP molecule desorbed from the surface. However, this basic description does not explain the observation that the measured TH of IBPs is a function of their concentration in solution, typically proportional to the square root of the concentration (Wen and Laursen 1992b). If the irreversibility assumption is dismissed, such proportionality can be supported by assuming that the surface concentration of the IBP on ice is a result of an equilibrium between adsorption and desorption of the IBPs. Several equilibrium models have been suggested, where the density of IBPs on the ice surface is a function of the concentration of the IBPs in solution. The distance between molecules can be calculated from the surface density and is related to the TH by the Gibbs–Thomson equation (Yeh and Feeney 1996); but in some instances, surface density was related to TH without justification (Jorov et al. 2004; Liu and Li 2006).

The irreversibility of IBP binding to ice was tested by a series of experiments using fluorescently labeled IBPs (Celik et al. 2013; Drori et al. 2014b, 2015; Haleva et al. 2016; Meister et al. 2018; Pertaya et al. 2007b; Zepeda et al. 2008). Fluorescence recovery after photobleaching showed that type III AFP molecules are bound to an ice crystal surface and do not exchange with the surrounding protein in solution during 20 h of observation. This finding led to the estimation of the fastest IBP–ice

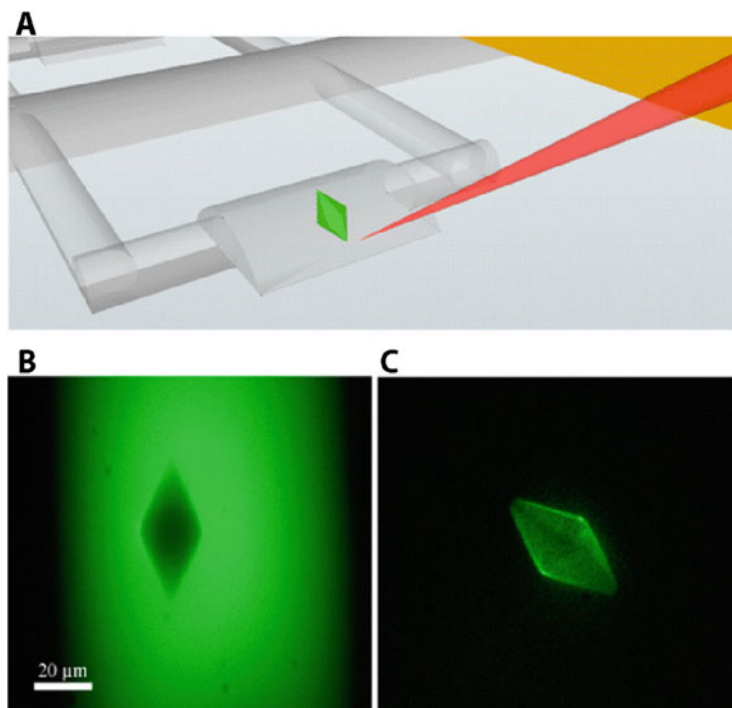


**Fig. 4.6** Ice crystal in a microfluidic device. (a) An illustration of an ice crystal coated by GFP-tagged IBPs in a microfluidic channel. (b–c) Imaging of an ice crystal coated with GFP-labeled type III AFP in the microfluidic channel. The green color is the fluorescent signal of the GFP-labeled protein. (b) The ice crystal is held in a solution containing protein. The crystal is darker than the solution because it does not contain protein inside it. (c) The same crystal in (b) after washing the protein solution from the microfluidic channel. The labeled protein remains bound to the ice surface. Reprinted (adapted) with permission from (Drori et al. 2015) Copyright (2015) American Chemical Society

off-rate being a week<sup>-1</sup> and the slowest being infinity—essentially quasi-permanent binding (Pertaya et al. 2007b). Experiments in microfluidic devices that allow the exchange of the solution around ice crystals provided further support for irreversible binding. Ice crystals coated with IBPs were washed such that the solution around the crystals was replaced with solution containing almost no protein. It was shown that the fluorescence signal from the ice surfaces was not reduced after the washing (Fig. 4.6) (Celik et al. 2013; Drori et al. 2014b, 2015). Further still, freezing hysteresis by hyperactive AFP (*TmAFP*) was maintained even when the only proteins in the system were those on the ice surface and not in the solution.

In two situations where fluorescently labeled IBPs were allowed to accumulate on an ice crystal surface, after which ice growth was forced on the system, the fluorescence signal was lost or reduced. With a mixture of AFGPs 4 to 6 (70% being AFGP 6) that were labeled at the N terminus with fluorescein isothiocyanate, the fluorescence on the ice surface vanished when a layer of ice overgrew the area

that was exposed to the AFPs (Zepeda et al. 2008). However, with hyperactive IBPs, although the fluorescence of their GFP tags was greatly reduced when a layer of ice overgrew the area where the protein had accumulated, the fluorescence signal returned when the newly formed ice layer was melted back to the point of accumulation (Haleva et al. 2016). The most likely explanation for this phenomenon is that overgrowth by ice caused enough distorting of the protein fluorophore to spoil its fluorescence, and that when the ice melted, the structural stress in the GFP moiety was relieved and the fluorescence was restored. It seems unlikely that this same explanation can account for the loss of fluorescence when the tagged AFGP area was overgrown by ice. While this experiment might suggest that the AFGPs are reversible binders, it might also indicate that under the condition of ice growth used in that experiment, the AFGPs were pushed off the ice rather than overgrown. On the contrary, other experiments with AFGPs support their irreversible binding to ice (Meister et al. 2018). Overall, these results offer additional support for the irreversible binding of hyperactive AFPs and hint at irreversible binding of other IBPs as well.

Irreversible binding of IBPs to ice is the basis for ice affinity purification (Adar et al. 2018; Garnham et al. 2010; Kuiper et al. 2003; Marshall et al. 2004b, 2016), ice etching (Knight et al. 1991, 2001), and the FIPA modification of ice etching (Basu et al. 2014; Garnham et al. 2010). In these methods ice is grown slowly in solutions of IBPs, around chilled cold fingers, or on a shell of ice formed around a round-bottomed flask (Marshall et al. 2016), or on vertical cold plate on which the solution is flowing (Adar et al. 2018). The slowly growing ice front rejects all solutes except IBPs that are incorporated into it. Thus, the binding of IBPs to ice allows them to resist rejection by the growing ice layers. Overall, the experimental results indicate that most IBPs, at least the moderate and hyperactive ones, irreversibly bind to ice surfaces.

To reconcile the concept of irreversible ice binding with the dependence of TH on protein solution concentration, Kristiansen and Zachariassen suggested a two-step binding model. In the first step, the surface densities of the proteins equilibrate near the melting point at the ice–water interface. Upon cooling, the IBPs are “locked” to their position on the ice surface (Kristiansen and Zachariassen 2005). However, this explanation does not have experimental support. For example, it was shown that in addition to ice growth arrest, IBPs also inhibit ice melting (Celik et al. 2010; Cziko et al. 2014; Knight and DeVries 1989). Therefore, supercooling is not necessary for “locking” IBP molecules to ice surfaces, and the irreversibility model is relevant at temperatures close to the melting point. Moreover, fluorescence measurements showed that IBPs accumulate on the ice surface at temperatures lower than the melting point (Drori et al. 2014a, 2015; Haleva et al. 2016; Takamichi et al. 2007; Zepeda et al. 2008). Recent concepts suggest the coexistence of irreversible binding and the measured dependence of TH on protein solution concentration are related to the kinetics of IBP binding to ice surfaces, as discussed in the next session on the binding kinetics of IBPs to ice.



## 4.12 The Dynamics of Binding

If TH stems from a surface phenomenon, one should expect that the dynamics of the adsorption process would have a crucial role (Burcham et al. 1986; Kubota 2011). Experiments to detect accumulation of AFGPs on ice surfaces were first attempted by ellipsometry and yielded evidence that there is a time scale of minutes for accumulation of AFGPs to ice surfaces (Wilson 1993). Chapsky and Rubinsky used a unidirectional capillary-based TH measurement of type I AFP to evaluate the dynamic nature of the TH activity. In these experiments, ice propagation in capillaries was monitored in a controlled-temperature gradient. The authors found that in the presence of the AFPs, ice stops growing at a temperature just below the melting point, and resumes growing at lower temperatures. This additional supercooling needed for growth was time dependent. The TH increased over time up to fivefold when the ice was held at sub-melting temperatures for an hour without growth. The authors concluded that the observed time dependence is too slow to be limited by the binding kinetics, and the increase in TH was a result of rearrangement of the surface of the ice and the proteins that bind to it (Chapsky and Rubinsky 1997). The long incubation time of ice crystals in solutions of type III AFP in a nanoliter osmometer was found to increase the thermal hysteresis up to 2.5-fold over a period of 2 h if the crystal was held at high supercooling (close to the freezing point) (Takamichi et al. 2007). Fig. 4.7a represents the course of such an experiment using a nanoliter osmometer. A much stronger time dependence was found for hyperactive AFPs, as shown in Fig. 4.7b (Braslavsky and Drori 2013; Drori et al. 2014a; Xiao et al. 2014). When the crystal was allowed to incubate just below the melting point for ~ 16 h in a solution of a hyperactive AFP, TH increased 40-fold over the value obtained after just a few seconds incubation (Drori et al. 2014a) (Fig. 4.7b). On the contrary, moderate AFPs such as type III AFP achieved most of their full activity even at short exposure times of a few seconds (Drori et al. 2014a; Takamichi et al. 2007). The difference in the dynamic response between hyperactive and moderate AFPs was shown also in sonocrystallization experiments, in which a 1-ml IBP solution was cooled to several degrees below the melting point before it was nucleated by an acoustic pulse. After nucleation, the solution stabilized at a temperature lower than the melting point, and the difference from the melting point was determined as the TH. It was shown that the TH values of type III AFP were similar when measured by a nanoliter osmometer and sonocrystallization, but hyperactive AFP had a very small TH values in the sonocrystallization assay compared to the nanoliter osmometer (Olijve et al. 2016).

Measurements of the fluorescence signal from labeled IBPs on ice crystals allow determination of their accumulation rates as well as identification of the planes on which IBPs gather (Celik et al. 2010; Drori et al. 2014a, b, 2015; Haleva et al. 2016; Kaleda et al. 2019; Pertaya et al. 2008). It was shown that hyperactive AFPs such as *Tm*AFP, *sbw*AFP, *Mp*IBP-RIV, and *Ri*AFP, accumulate on the basal plane of ice crystals, in addition to other planes. For some of the hyperactive AFPs, the accumulation continues for hours, with no clear end point (Drori et al. 2014a, b; Haleva

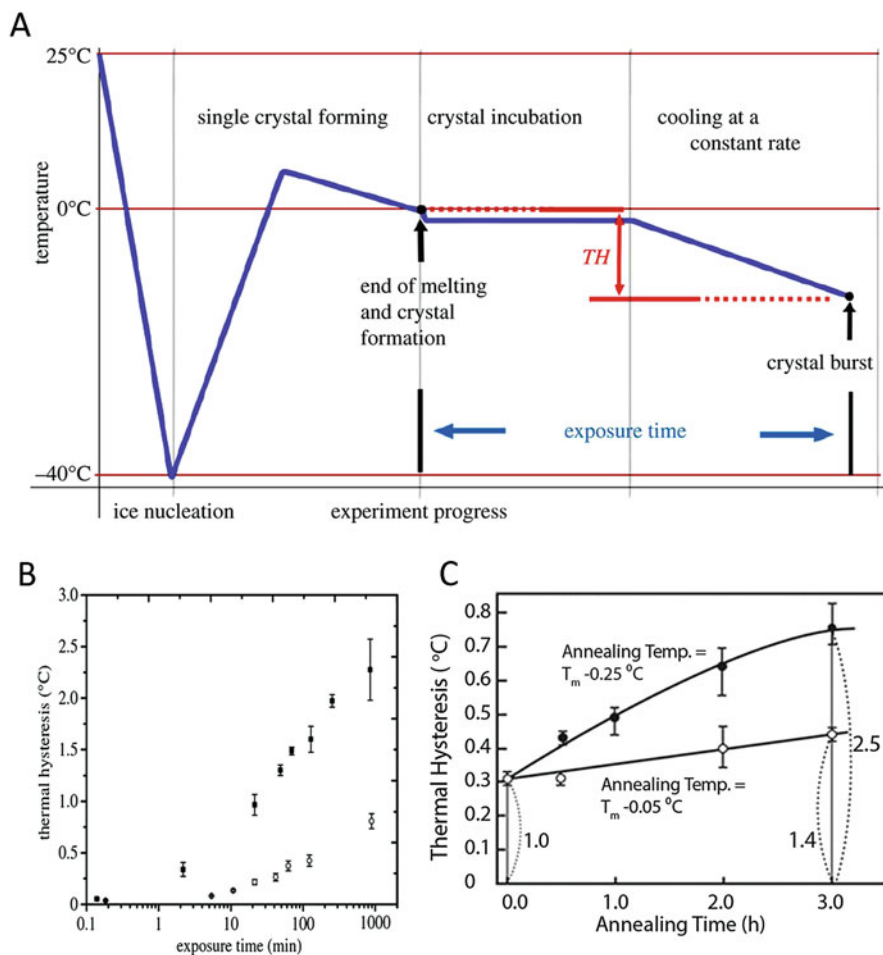


**Fig. 4.7** Time dependence of TH activity. (a) Representation of the experimental procedure conducted using a nanoliter osmometer. (b) TH as a function of the exposure time for a solution of 4  $\mu\text{M}$  (open circles) and 8  $\mu\text{M}$  (filled squares) sbwAFP annealed at  $-0.05^\circ\text{C}$  below the melting point (Modified from (Drori et al. 2014a)). (c) TH as a function of the exposure time for a solution of 100  $\mu\text{M}$  of type III AFP (nfeAFP) annealed at  $-0.25^\circ\text{C}$  (filled circles) or  $-0.05^\circ\text{C}$  (open circles) below the melting point (reprinted from (Takamichi et al. 2007). Copyright (2007) WILEY)

et al. 2016; Pertaya et al. 2008). In order to fit the fluorescence intensity as a function of a time scale that spans from few seconds to an hour, three exponents were necessary (Drori et al. 2014a). In contrast, the accumulation of moderate AFPs on non-basal planes fits a single exponent, with an on-rate constant of  $K_{\text{on}} = 0.008 \mu\text{M}^{-1} \text{S}^{-1}$ . Using this rate constant, we can calculate for a solution with an AFP concentration of  $C = 50 \mu\text{M}$ , for example, a typical time for accumulation of the proteins as  $\tau = \frac{1}{CK_{\text{on}}} = 2.5 \text{ s}$ . Thus the observed weak dependence of TH

of type III AFP on much longer times of exposure is probably not related to the rate of accumulation of the proteins on the ice surface (Drori et al. 2014a).

A theory developed by Knight and DeVries based on experiments on ice growth in the presence of AFGPs gives a good explanation for the dependence of TH on the concentration of type III AFPs (Knight and DeVries 2009). According to this theory, the TH limit is determined by the ability of AFP to kinetically block new ice that grows on the unprotected face of the ice crystal—typically the basal plane for moderately active AFPs. The AFPs bind irreversibly to ice prism and pyramidal planes, but additional AFPs are needed in solution in order to inhibit further growth that may emerge from the basal plane. In accordance with this theory, experiments by Drori et al. using type III AFP in microfluidic devices showed that when the solution around protein-bound ice crystals was exchanged with a solution containing only traces of protein, the originally bound proteins stayed on the ice (Fig. 4.6), but the TH was somewhat reduced (Drori et al. 2015).

If the observed solution concentration dependence stems from IBP adsorption rate and not from the density of accumulated protein on the ice surface, the observed square root dependence of the solution concentration on TH remains an open question. Sander and Tkachenko developed a kinetic pinning theory for the inhibition of ice growth by IBPs. They assumed that the binding is irreversible, with an option for the proteins to be engulfed by the growing ice if the angle of contact between the ice and the protein becomes too large. Under these assumptions, they showed that for a certain protein concentration and supercooling, the velocity of the ice growth comes to a halt. They obtained a square root relation between the TH and the protein concentration (Sander and Tkachenko 2004).

The combination of the theories by Sander and Knight gives a plausible explanation for the experimental findings for the moderate IBPs that do not bind to ice basal planes. However, there is clear experimental evidence that hyperactive AFPs bind to basal planes and inhibit their growth, as discussed in Sect. 4.4. It was also shown that the TH of hyperactive AFPs was not diminished when there was no protein in solution (Celik et al. 2013), as opposed to type III AFP (Drori et al. 2015). The observation that the TH increases with longer exposure times of the ice to the proteins (Drori et al. 2014a), the insensitivity of the TH to the protein concentration in solution (Celik et al. 2013), as well as the long accumulation times of hyperactive AFPs (Drori et al. 2014a; Haleva et al. 2016), led to the conclusion that there is a direct connection between the surface protein concentration and the measured TH in the case of AFPs that bind the basal planes in addition to prism planes. It is interesting to note that while TH as a function of concentration of a variety of moderate AFPs can be well matched with the kinetic pinning model, there is not a good match for hyperactive AFPs (Chasnitsky and Braslavsky 2019; Kozuch et al. 2018). Estimation of the surface density of the proteins and the TH as a function of time is in agreement with the basic inverse relation between TH and molecules distance as in the Gibbs–Thomson equation. Still, TH measurements deviate from the TH calculated using this equation. Drori et al. measured a distance of a few nanometers between bound protein molecules on an ice surface (Drori et al. 2014b). The calculated TH for such surface concentration is much higher. This disagreement

was noted before and was speculated to be related to the angle of contact between the proteins and the ice (Acker et al. 2001; Drori et al. 2014b; Higgins and Karlsson 2013; Karlsson et al. 2019; Mazur 1965). Another aspect in evaluating the relationship between molecule distance separation and TH is the arbitrary assumption that the proteins are evenly distributed on the ice surface. This assumption can be modified to a random distribution (Hansen-Goos et al. 2014).

While the advance in the understanding of the activity of IBPs is significant, many aspects remain to be explained. For example, what is the microscopic arrangement of IBPs on a particular ice plane? Why do hyperactive AFPs continue to accumulate on the ice surface for such a long time? What determines the recrystallization inhibition limits? What is the correlation between ice recrystallization inhibition and TH? To answer these and further questions, additional experimental approaches with higher resolution should be implemented, along with elaborate simulations of ice, water, and IBPs.

### 4.13 Conclusions

IBPs from many biological kingdoms have been characterized. New IBPs with novel structures await discovery, and the range of their specific activities and natural functions may yet increase. Clearly, we have not yet plumbed the complexity of this protein class. Many theories regarding the ice-binding mechanism of various types of IBPs have been advanced and ruled out by experiments. In this chapter, we discussed the advances in the understanding of IBP structures and their mechanism of ice recognition, both for specific IBP types and more generally for all IBPs. The most plausible mechanism that explains the way IBPs interact with ice is the “anchored clathrate water” model. Despite the dramatic differences between IBP types, this theory can apply to all IBPs. Nevertheless, the way each IBP holds water molecules on its ice-binding face, and the number of water molecules in the clathrate can be type specific.

**Acknowledgments** This work was supported by grants from the Canadian Institutes of Health Research (P.L.D.) and the Israel Science Foundation (I.B.). P.L.D. holds the Canada Research Chair in Protein Engineering.

### References

- Achenbach JC, Ewart KV (2002) Structural and functional characterization of a C-type lectin-like antifreeze protein from rainbow smelt (*Osmerus mordax*). *Eur J Biochem* 269:1219–1226
- Acker JP, Elliott JAW, McGann LE (2001) Intercellular ice propagation: experimental evidence for ice growth through membrane pores. *Biophys J* 81:1389–1397
- Adar C, Sirotinskaya V, Bar Dolev M, Friehmann T, Braslavsky I (2018) Falling water ice affinity purification of ice-binding proteins. *Sci Rep* 8:11046

- Antson AA, Smith DJ, Roper DI, Lewis S, Caves LSD, Verma CS, Buckley SL, Lillford PJ, Hubbard RE (2001) Understanding the mechanism of ice binding by type III antifreeze proteins. *J Mol Biol* 305:875–889
- Baardsnes J, Davies PL (2002) Contribution of hydrophobic residues to ice binding by fish type III antifreeze protein. *Biochim Biophys Acta* 1601:49–54
- Baardsnes J, Kondejewski LH, Hodges RS, Chao H, Kay C, Davies PL (1999) New ice-binding face for type I antifreeze protein. *FEBS Lett* 463:87–91
- Baardsnes J, Kuiper MJ, Davies PL (2003) Antifreeze protein dimer: when two ice-binding faces are better than one. *J Biol Chem* 278:38942–38947
- Bar Dolev M, Celik Y, Wettlaufer JS, Davies PL, Braslavsky I (2012) New insights into ice growth and melting modifications by antifreeze proteins. *J R Soc Interface* 9:3249–3259
- Bar Dolev M, Bernheim R, Guo SQ, Davies PL, Braslavsky I (2016a) Putting life on ice: bacteria that bind to frozen water. *J R Soc Interface* 13:20160210
- Bar Dolev M, Braslavsky I, Davies PL (2016b) Ice-binding proteins and their function. *Annu Rev Biochem* 85:515–542
- Bar M, Celik Y, Fass D, Braslavsky I (2008a) Interactions of beta-helical antifreeze protein mutants with ice. *Cryst Growth Des* 8:2954–2963
- Bar M, Scherf T, Fass D (2008b) Two-dimensional surface display of functional groups on a beta-helical antifreeze protein scaffold. *Protein Eng Des Sel* 21:107–114
- Basu K, Garnham CP, Nishimiya Y, Tsuda S, Braslavsky I, Davies P (2014) Determining the ice-binding planes of antifreeze proteins by fluorescence-based Ice plane affinity. *J Vis Exp* 83:e51185
- Basu K, Graham LA, Campbell RL, Davies PL (2015) Flies expand the repertoire of protein structures that bind ice. *Proc Natl Acad Sci USA* 112:737–742
- Basu K, Wasserman SS, Jeronimo PS, Graham LA, Davies PL (2016) Intermediate activity of midge antifreeze protein is due to a tyrosine-rich ice-binding site and atypical ice plane affinity. *FEBS J* 283:1504–1515
- Berger T, Meister K, DeVries AL, Eves R, Davies PL, Drori R (2019) Synergy between antifreeze proteins is driven by complementary ice-binding. *J Am Chem Soc* 141:19144–19150
- Bissoyi A, Reicher N, Chasnitsky M, Arad S, Koop T, Rudich Y, Braslavsky I (2019) Ice nucleation properties of ice-binding proteins from snow fleas. *Biomol Ther* 9:532
- Braslavsky I, Drori R (2013) LabVIEW-operated novel nanoliter osmometer for ice binding protein investigations. *J Vis Exp* 72:e4189
- Burcham TS, Osuga DT, Yeh Y, Feeney RE (1986) A kinetic description of antifreeze glycoprotein activity. *J Biol Chem* 261:6390–6397
- Can O, Holland NB (2011) Conjugation of type I antifreeze protein to polyallylamine increases thermal hysteresis activity. *Bioconjug Chem* 22:2166–2171
- Celik Y, Graham LA, Mok YF, Bar M, Davies PL, Braslavsky I (2010) Superheating of ice crystals in antifreeze protein solutions. *Proc Natl Acad Sci USA* 107:5423–5428
- Celik Y, Drori R, Pertaya-Braun N, Altan A, Barton T, Bar-Dolev M, Groisman A, Davies PL, Braslavsky I (2013) Microfluidic experiments reveal that antifreeze proteins bound to ice crystals suffice to prevent their growth. *Proc Natl Acad Sci USA* 110:1309–1314
- Chao H, Davies P, Sonnichsen F, Sykes B (1993) Solution structure of a novel, non-helical type-iii antifreeze protein via proline replacement. *Protein Eng* 6:31–31
- Chao H, Sonnichsen FD, DeLuca CI, Sykes BD, Davies PL (1994) Structure-function relationship in the globular type III antifreeze protein: identification of a cluster of surface residues required for binding to ice. *Protein Sci* 3:1760–1769
- Chao H, Hodges RS, Kay CM, Gauthier SY, Davies PL (1996) A natural variant of type I antifreeze protein with four ice-binding repeats is a particularly potent antifreeze. *Protein Sci* 5:1150–1156
- Chao H, Houston ME, Hodges RS, Kay CM, Sykes BD, Loewen MC, Davies PL, Sönnichsen FD (1997) A diminished role for hydrogen bonds in antifreeze protein binding to Ice. *Biochemistry* 36:14652–14660

- Chapsky L, Rubinsky B (1997) Kinetics of antifreeze protein-induced ice growth inhibition. *FEBS Lett* 412:241–244
- Chasnitsky M, Braslavsky I (2019) Ice-binding proteins and the applicability and limitations of the kinetic pinning model. *Philos Trans R Soc A Math Phys Eng Sci* 377:20180391
- Chen L, DeVries AL, Cheng CH (1997) Convergent evolution of antifreeze glycoproteins in Antarctic notothenioid fish and Arctic cod. *Proc Natl Acad Sci USA* 94:3817–3822
- Cheng CHC, DeVries AL (1989) Structures of antifreeze peptides from the antarctic eel pout, *Austrolycichthys-Brachycephalus*. *Biochim Biophys Acta* 997:55–64
- Chou K-C (1992) Energy-optimized structure of antifreeze protein and its binding mechanism. *J Mol Biol* 223:509–517
- Cziko PA, DeVries AL, Evans CW, Cheng C-HC (2014) Antifreeze protein-induced superheating of ice inside Antarctic notothenioid fishes inhibits melting during summer warming. *Proc Natl Acad Sci USA* 111:14583–14588
- Davies PL (2014) Ice-binding proteins: a remarkable diversity of structures for stopping and starting ice growth. *Trends Biochem Sci* 39:548–555
- Davies PL, Baardsnes J, Kuiper MJ, Walker VK (2002) Structure and function of antifreeze proteins. *Philos Trans R Soc Lond Ser B Biol Sci* 357:927–935
- DeVries AL, Price TJ (1984) Role of glycopeptides and peptides in inhibition of crystallization of water in polar fishes [and discussion]. *Philos Trans R Soc Lond B Biol Sci* 304:575–588
- DeLuca CI, Chao H, Sonnichsen FD, Sykes BD, Davies PL (1996) Effect of type III antifreeze protein dilution and mutation on the growth inhibition of ice. *Biophys J* 71:2346–2355
- DeLuca CI, Comley R, Davies PL (1998) Antifreeze proteins bind independently to ice. *Biophys J* 74:1502–1508
- DeVries AL, Lin Y (1977) Structure of a peptide antifreeze and mechanism of adsorption to ice. *Biochim Biophys Acta* 495:388–392
- DeVries AL, Wohlschlag DE (1969) Freezing resistance in some Antarctic fishes. *Science* 163:1073–1075
- Doucet D, Tyshenko MG, Kuiper MJ, Graether SP, Sykes BD, Daugulis AJ, Davies PL, Walker VK (2000) Structure–function relationships in spruce budworm antifreeze protein revealed by isoform diversity. *Eur J Biochem* 267:6082–6088
- Drori R, Celik Y, Davies PL, Braslavsky I (2014a) Ice-binding proteins that accumulate on different ice crystal planes produce distinct thermal hysteresis dynamics. *J R Soc Interface* 11:20140526
- Drori R, Davies PL, Braslavsky I (2014b) Experimental correlation between thermal hysteresis activity and the distance between antifreeze proteins on an ice surface. *RSC Adv* 5:7848
- Drori R, Davies PL, Braslavsky I (2015) When are antifreeze proteins in solution essential for ice growth inhibition? *Langmuir* 31:5805–5811
- Duman JG (2001) Antifreeze and ice nucleator proteins in terrestrial arthropods. *Annu Rev Physiol* 63:327–357
- Duman JG, DeVries AL (1976) Isolation, characterization, and physical properties of protein antifreezes from the winter flounder, *Pseudopleuronectes americanus*. *Comp Biochem Physiol B* 54:375–380
- Duman JG, Li N, Verleye D, Goetz FW, Wu DW, Andorfer CA, Benjamin T, Parmelee DC (1998) Molecular characterization and sequencing of antifreeze proteins from larvae of the beetle *Dendroides canadensis*. *J Comp Physiol B Biochem Syst Environ Physiol* 168:225–232
- Ebbinghaus S, Meister K, Born B, DeVries AL, Gruebele M, Havenith M (2010) Antifreeze glycoprotein activity correlates with long-range protein–water dynamics. *J Am Chem Soc* 132:12210–12211
- Ebbinghaus S, Meister K, Prigozhin MB, DeVries AL, Havenith M, Dzubiella J, Gruebele M (2012) Functional importance of short-range binding and long-range solvent interactions in helical antifreeze peptides. *Biophys J* 103:L20–L22
- Eickhoff L, Dreischmeier K, Zipori A, Sirotinskaya V, Adar C, Reicher N, Braslavsky I, Rudich Y, Koop T (2019) Contrasting behavior of antifreeze proteins: ice growth inhibitors and ice nucleation promoters. *J Phys Chem Lett* 10:966–972



- Evans RP, Fletcher GL (2001) Isolation and characterization of type I antifreeze proteins from Atlantic snailfish (*Liparis atlanticus*) and dusky snailfish (*Liparis gibbus*). *Biochim Biophys Acta* 1547:235–244
- Ewart KV, Fletcher GL (1990) Isolation and characterization of antifreeze proteins from smelt (*Osmerus-Mordax*) and atlantic herring (*Clupea-Harengus-Harengus*). *Can J Zool* 68:1652–1658
- Feeney RE, Burcham TS, Yeh Y (1986) Antifreeze glycoproteins from polar fish blood. *Annu Rev Biophys Chem* 15:59–78
- Gallagher KR, Sharp KA (2003) Analysis of thermal hysteresis protein hydration using the random network model. *Biophys Chem* 105:195–209
- Garnham CP, Gilbert JA, Hartman CP, Campbell RL, Laybourn-Parry J, Davies PL (2008) A Ca<sup>2+</sup>-dependent bacterial antifreeze protein domain has a novel beta-helical ice-binding fold. *Biochem J* 411:171–180
- Garnham CP, Natarajan A, Middleton AJ, Kuiper MJ, Braslavsky I, Davies PL (2010) Compound ice-binding site of an antifreeze protein revealed by mutagenesis and fluorescent tagging. *Biochemistry* 49:9063–9071
- Garnham CP, Campbell RL, Davies PL (2011a) Anchored clathrate waters bind antifreeze proteins to ice. *Proc Natl Acad Sci USA* 108:7363–7367
- Garnham CP, Campbell RL, Walker VK, Davies PL (2011b) Novel dimeric beta-helical model of an ice nucleation protein with bridged active sites. *BMC Struct Biol* 11:36
- Garnham CP, Nishimiya Y, Tsuda S, Davies PL (2012) Engineering a naturally inactive isoform of type III antifreeze protein into one that can stop the growth of ice. *FEBS Lett* 586:3876–3881
- Gauthier SY, Scotter AJ, Lin FH, Baardsnes J, Fletcher GL, Davies PL (2008) A re-evaluation of the role of type IV antifreeze protein. *Cryobiology* 57:292–296
- Govindarajan AG, Lindow SE (1988) Size of bacterial ice-nucleation sites measured in situ by radiation inactivation analysis. *Proc Natl Acad Sci USA* 85:1334–1338
- Grabowska J, Kuffel A, Zielkiewicz J (2016) Structure of solvation water around the active and inactive regions of a type III antifreeze protein and its mutants of lowered activity. *J Chem Phys* 145:075101
- Graether SP, Jia Z (2001) Modeling *Pseudomonas syringae* ice-nucleation protein as a beta-helical protein. *Biophys J* 80:1169–1173
- Graether SP, Kuiper MJ, Gagne SM, Walker VK, Jia Z, Sykes BD, Davies PL (2000) Beta-helix structure and ice-binding properties of a hyperactive antifreeze protein from an insect. *Nature* 406:325–328
- Graham LA, Davies PL (2005) Glycine-rich antifreeze proteins from snow fleas. *Science* 310:461
- Graham LA, Liou YC, Walker VK, Davies PL (1997) Hyperactive antifreeze protein from beetles. *Nature* 388:727–728
- Graham LA, Hobbs RS, Fletcher GL, Davies PL (2013) Helical antifreeze proteins have independently evolved in fishes on four occasions. *PLoS One* 8:e81285
- Green RL, Corotto LV, Warren GJ (1988) Deletion mutagenesis of the ice nucleation gene from *Pseudomonas syringae* S203. *Mol Gen Genet* 215:165–172
- Guo S, Garnham CP, Whitney JC, Graham LA, Davies PL (2012) Re-evaluation of a bacterial antifreeze protein as an adhesin with ice-binding activity. *PLoS One* 7:e48805
- Guo S, Stevens CA, Vance TDR, Olijve LLC, Graham LA, Campbell RL, Yazdi SR, Escobedo C, Bar-Dolev M, Yashunsky V et al (2017) Structure of a 1.5-MDa adhesin that binds its Antarctic bacterium to diatoms and ice. *Sci Adv* 3:e1701440
- Guriansherman D, Lindow SE (1993) Bacterial ice nucleation – significance and molecular-basis. *FASEB J* 7:1338–1343
- Hakim A, Nguyen JB, Basu K, Zhu DF, Thakral D, Davies PL, Isaacs FJ, Modis Y, Meng W (2013) Crystal structure of an insect antifreeze protein and its implications for ice binding. *J Biol Chem* 288(17):12295–12304

- Haleva L, Celik Y, Bar-Dolev M, Pertaya-Braun N, Kaner A, Davies PL, Braslavsky I (2016) Microfluidic cold-finger device for the investigation of ice-binding proteins. *Biophys J* 111:1143–1150
- Hansen-Goos H, Thomson ES, Wettlaufer JS (2014) On the edge of habitability and the extremes of liquidity. *Planet Space Sci* 98:169–181
- Haymet ADJ, Ward LG, Harding MM, Knight CA (1998) Valine substituted winter flounder ‘antifreeze’: preservation of ice growth hysteresis. *FEBS Lett* 430:301–306
- Haymet ADJ, Ward LG, Harding MM (1999) Winter flounder “antifreeze” proteins: synthesis and ice growth inhibition of analogues that probe the relative importance of hydrophobic and hydrogen-bonding interactions. *J Am Chem Soc* 121:941–948
- Hayward JA, Haymet ADJ (2001) The ice/water interface: molecular dynamics simulations of the basal, prism, {20(2)over-bar1}, and {2(11)over-bar0} interfaces of ice Ih. *J Chem Phys* 114:3713–3726
- Hew CL, Joshi S, Wang N-C, Kao M-H, Ananthanarayanan VS (1985) Structures of shorthorn sculpin antifreeze polypeptides. *Eur J Biochem* 151:167–172
- Hew CL, Wang NC, Joshi S, Fletcher GL, Scott GK, Hayes PH, Buettner B, Davies PL (1988) Multiple genes provide the basis for antifreeze protein diversity and dosage in the ocean pout, *Macrozoarces americanus*. *J Biol Chem* 263:12049–12055
- Hew CL, Davies PL, Fletcher G (1992) Antifreeze protein gene transfer in Atlantic salmon. *Mol Mar Biol Biotechnol* 1:309–317
- Higgins AZ, Karlsson JOM (2013) Effects of intercellular junction protein expression on intracellular ice formation in mouse insulinoma cells. *Biophys J* 105:2006–2015
- Hobbs RS, Shears MA, Graham LA, Davies PL, Fletcher GL (2011) Isolation and characterization of type I antifreeze proteins from cunner, *Tautoglabrus adspersus*, order Perciformes. *FEBS J* 278:3699–3710
- Holland NB, Nishimiya Y, Tsuda S, Sönnichsen FD (2008) Two domains of RD3 antifreeze protein diffuse independently. *Biochemistry* 47:5935–5941
- Howard EI, Blakeley MP, Haertlein M, Haertlein IP, Mitschler A, Fisher SJ, Siah AC, Salvay AG, Popov A, Dieckmann CM et al (2011) Neutron structure of type-III antifreeze protein allows the reconstruction of AFP–ice interface. *J Mol Recognit* 24:724–732
- Hsiao KC, Cheng CH, Fernandes IE, Detrich HW, DeVries AL (1990) An antifreeze glycopeptide gene from the Antarctic cod *Notothenia coriiceps* neglecta encodes a polyprotein of high peptide copy number. *Proc Natl Acad Sci USA* 87:9265–9269
- Hudait A, Moberg DR, Qiu Y, Odendahl N, Paesani F, Molinero V (2018) Preordering of water is not needed for ice recognition by hyperactive antifreeze proteins. *Proc Natl Acad Sci USA* 115:8266–8271
- Jia Z, Davies PL (2002) Antifreeze proteins: an unusual receptor-ligand interaction. *Trends Biochem Sci* 27:101–106
- Jia Z, DeLuca CI, Chao H, Davies PL (1996) Structural basis for the binding of a globular antifreeze protein to ice. *Nature* 384:285–288
- Jorov A, Zhorov BS, Yang DSC (2004) Theoretical study of interaction of winter flounder antifreeze protein with ice. *Protein Sci* 13:1524–1537
- Kaleda A, Haleva L, Sarusi G, Pinsky T, Mangiagalli M, Bar Dolev M, Lotti M, Nardini M, Braslavsky I (2019) Saturn-shaped ice burst pattern and fast basal binding of an ice-binding protein from an Antarctic bacterial consortium. *Langmuir* 35:7337–7346
- Karlsson JOM, Braslavsky I, Elliott JAW (2019) Protein-water-ice contact angle. *Langmuir* 35:7383–7387
- Kawahara H (2002) The structures and functions of ice crystal-controlling proteins from bacteria. *J Biosci Bioeng* 94:492–496
- Kawahara H (2013) Characterizations of functions of biological materials having controlling-ability against ice crystal growth. In: Sukarno F (ed) *Advanced topics on crystal growth*. InTech, Rijeka, pp 119–143
- Kieft TL (1988) Ice nucleation activity in lichens. *Appl Environ Microbiol* 54:1678–1681

- King NP, Bale JB, Sheffler W, McNamara DE, Gonen S, Gonen T, Yeates TO, Baker D (2014) Accurate design of co-assembling multi-component protein nanomaterials. *Nature* 510:103–108
- Knight CA, DeVries AL (1989) Melting inhibition and superheating of ice by an antifreeze glycopeptide. *Science* 245:505–507
- Knight CA, DeVries AL (2009) Ice growth in supercooled solutions of a biological “antifreeze”, AFGP 1-5: an explanation in terms of adsorption rate for the concentration dependence of the freezing point. *Phys Chem Chem Phys* 11:5749–5761
- Knight CA, Wierzbicki A (2001) Adsorption of biomolecules to ice and their effects upon ice growth. 2. A discussion of the basic mechanism of “antifreeze” phenomena. *Cryst Growth Des* 1:439–446
- Knight CA, Cheng CC, DeVries AL (1991) Adsorption of alpha-helical antifreeze peptides on specific ice crystal-surface planes. *Biophys J* 59:409–418
- Knight CA, Driggers E, DeVries AL (1993) Adsorption to ice of fish antifreeze glycopeptide-7 and glycopeptide-8. *Biophys J* 64:252–259
- Knight CA, Wierzbicki A, Laursen RA, Zhang W (2001) Adsorption of biomolecules to ice and their effects upon ice growth. 1. Measuring adsorption orientations and initial results. *Cryst Growth Des* 1:429–438
- Kobashigawa Y, Nishimiya Y, Miura K, Ohgiya S, Miura A, Tsuda S (2005) A part of ice nucleation protein exhibits the ice-binding ability. *FEBS Lett* 579:1493–1497
- Kondo H, Hanada Y, Sugimoto H, Hoshino T, Garnham CP, Davies PL, Tsuda S (2012) Ice-binding site of snow mold fungus antifreeze protein deviates from structural regularity and high conservation. *Proc Natl Acad Sci USA* 109:9360–9365
- Kozuch DJ, Stillingner FH, Debenedetti PG (2018) Combined molecular dynamics and neural network method for predicting protein antifreeze activity. *Proc Natl Acad Sci USA* 115:13252–13257
- Kristiansen E, Zachariassen KE (2005) The mechanism by which fish antifreeze proteins cause thermal hysteresis. *Cryobiology* 51:262–280
- Kristiansen E, Ramløv H, Højrup P, Pedersen SA, Hagen L, Zachariassen KE (2011) Structural characteristics of a novel antifreeze protein from the longhorn beetle *Rhagium inquisitor*. *Insect Biochem Mol Biol* 41:109–117
- Kristiansen E, Wilkens C, Vincents B, Friis D, Lorentzen AB, Jenssen H, Lobner-Olesen A, Ramlov H (2012) Hyperactive antifreeze proteins from longhorn beetles: some structural insights. *J Insect Physiol* 58:1502–1510
- Kubota N (2011) Effects of cooling rate, annealing time and biological antifreeze concentration on thermal hysteresis reading. *Cryobiology* 63:198–209
- Kuiper MJ, Lankin C, Gauthier SY, Walker VK, Davies PL (2003) Purification of antifreeze proteins by adsorption to ice. *Biochem Biophys Res Commun* 300:645–648
- Kumble KD, Demmer J, Fish S, Hall C, Corrales S, DeAth A, Elton C, Prestidge R, Luxmanan S, Marshall CJ et al (2008) Characterization of a family of ice-active proteins from the Ryegrass, *Lolium perenne*. *Cryobiology* 57:263–268
- Lee JH, Park AK, Do H, Park KS, Moh SH, Chi YM, Kim HJ (2012) Structural basis for antifreeze activity of ice-binding protein from arctic yeast. *J Biol Chem* 287:11460–11468
- Leinala EK, Davies PL, Doucet D, Tyshenko MG, Walker VK, Jia Z (2002) A beta-helical antifreeze protein isoform with increased activity – structural and functional insights. *J Biol Chem* 277:33349–33352
- Li XM, Trinh KY, Hew CL, Buettner B, Baenziger J, Davies PL (1985) Structure of an antifreeze polypeptide and its precursor from the ocean pout, *Macrozoarces-Americanus*. *J Biol Chem* 260:2904–2909
- Limmer DT (2016) Closer look at the surface of ice. *Proc Natl Acad Sci USA* 113:12347–12349
- Lin FH, Davies PL, Graham LA (2011) The Thr- and Ala-rich hyperactive antifreeze protein from inchworm folds as a flat silk-like beta-helix. *Biochemistry* 50:4467–4478

- Liou Y-C, Thibault P, Walker VK, Davies PL, Graham LA (1999) A complex family of highly heterogeneous and internally repetitive hyperactive antifreeze proteins from the beetle *Tenebrio molitor*. *Biochemistry* 38:11415–11424
- Liou YC, Tocilj A, Davies PL, Jia Z (2000) Mimicry of ice structure by surface hydroxyls and water of a beta-helix antifreeze protein. *Nature* 406:322–324
- Liu JJ, Li QZ (2006) Theoretical model of antifreeze protein-ice adsorption: binding of large ligands to a two-dimensional homogeneous lattice. *Chem Phys Lett* 422:67–71
- Liu Y, Li Z, Lin Q, Kosinski J, Seetharaman J, Bujnicki JM, Sivaraman J, Hew CL (2007) Structure and evolutionary origin of Ca<sup>2+</sup>-dependent herring type II antifreeze protein. *PLoS One* 2: e548
- Liu JJ, Qin YZ, Bar Dolev M, Celik Y, Wettlaufer JS, Braslavsky I (2012) Modelling the influence of antifreeze proteins on three-dimensional ice crystal melt shapes using a geometric approach. *Proc R Soc A Math Phys Eng Sci* 468:3311–3322
- Liu K, Wang C, Ma J, Shi G, Yao X, Fang H, Song Y, Wang J (2016) Janus effect of antifreeze proteins on ice nucleation. *Proc Natl Acad Sci USA* 113:14739–14744
- Loewen MC, Gronwald W, Sonnichsen FD, Sykes BD, Davies PL (1998) The ice-binding site of sea raven antifreeze protein is distinct from the carbohydrate-binding site of the homologous C-type lectin. *Biochemistry* 37:17745–17753
- Low WK, Lin Q, Stathakis C, Miao M, Fletcher GL, Hew CL (2001) Isolation and characterization of skin-type, type I antifreeze polypeptides from the longhorn sculpin, *Myoxocephalus octodecemspinosus*. *J Biol Chem* 276:11582–11589
- Madura JD, Baran K, Wierzbicki A (2000) Molecular recognition and binding of thermal hysteresis proteins to ice. *J Mol Recognit* 13:101–113
- Mahatabuddin S, Hanada Y, Nishimiya Y, Miura A, Kondo H, Davies PL, Tsuda S (2017) Concentration-dependent oligomerization of an alpha-helical antifreeze polypeptide makes it hyperactive. *Sci Rep* 7:42501
- Mahatabuddin S, Fukami D, Arai T, Nishimiya Y, Shimizu R, Shibazaki C, Kondo H, Adachi M, Tsuda S (2018) Polypentagonal ice-like water networks emerge solely in an activity-improved variant of ice-binding protein. *Proc Natl Acad Sci USA* 115:5456–5461
- Mangiagalli M, Sarusi G, Kaleda A, Bar Dolev M, Nardone V, Vena VF, Braslavsky I, Lotti M, Nardini M (2018) Structure of a bacterial ice binding protein with two faces of interaction with ice. *FEBS J* 285:1653–1666
- Marshall CB, Daley ME, Graham LA, Sykes BD, Davies PL (2002) Identification of the ice-binding face of antifreeze protein from *Tenebrio molitor*. *FEBS Lett* 529:261–267
- Marshall CB, Daley ME, Sykes BD, Davies PL (2004a) Enhancing the activity of a beta-helical antifreeze protein by the engineered addition of coils. *Biochemistry* 43:11637–11646
- Marshall CB, Tomczak MM, Gauthier SY, Kuiper MJ, Lankin C, Walker VK, Davies PL (2004b) Partitioning of fish and insect antifreeze proteins into ice suggests they bind with comparable affinity. *Biochemistry* 43:148–154
- Marshall CJ, Basu K, Davies PL (2016) Ice-shell purification of ice-binding proteins. *Cryobiology* 72:258–263
- Mazur P (1965) Role of cell membranes in freezing of yeast and other single cells. *Ann N Y Acad Sci* 125:658–676
- Meister K, Ebbinghaus S, Xu Y, Duman JG, DeVries A, Gruebele M, Leitner DM, Havenith M (2013) Long-range protein–water dynamics in hyperactive insect antifreeze proteins. *Proc Natl Acad Sci USA* 110:1617–1622
- Meister K, Strazdaite S, DeVries AL, Lotze S, Olijve LLC, Voets IK, Bakker HJ (2014) Observation of ice-like water layers at an aqueous protein surface. *Proc Natl Acad Sci USA* 111:17732–17736
- Meister K, Lotze S, Olijve LLC, DeVries AL, Duman JG, Voets IK, Bakker HJ (2015) Investigation of the ice-binding site of an insect antifreeze protein using sum-frequency generation spectroscopy. *J Phys Chem Lett* 6:1162–1167

- Meister K, DeVries AL, Bakker HJ, Drori R (2018) Antifreeze glycoproteins bind irreversibly to ice. *J Am Chem Soc* 140:9365–9368
- Middleton AJ, Marshall CB, Faucher F, Bar-Dolev M, Braslavsky I, Campbell RL, Walker VK, Davies PL (2012) Antifreeze protein from freeze-tolerant grass has a beta-roll fold with an irregularly structured ice-binding site. *J Mol Biol* 416:713–724
- Miura K, Ohgiya S, Hoshino T, Nemoto N, Suetake T, Miura A, Spyropoulos L, Kondo H, Tsuda S (2001) NMR analysis of type III antifreeze protein intramolecular dimer. Structural basis for enhanced activity. *J Biol Chem* 276:1304–1310
- Modig K, Qvist J, Marshall CB, Davies PL, Halle B (2010) High water mobility on the ice-binding surface of a hyperactive antifreeze protein. *Phys Chem Chem Phys* 12:10189–10197
- Mok YF, Lin FH, Graham LA, Celik Y, Braslavsky I, Davies PL (2010) Structural basis for the superior activity of the large isoform of snow flea antifreeze protein. *Biochemistry* 49:2593–2603
- Nishimiya Y, Sato R, Takamichi M, Miura A, Tsuda S (2005) Co-operative effect of the isoforms of type III antifreeze protein expressed in Notched-fin eelpout, *Zoarces elongatus* Kner. *FEBS J* 272:482–492
- Nishimiya Y, Kondo H, Takamichi M, Sugimoto H, Suzuki M, Miura A, Tsuda S (2008) Crystal structure and mutational analysis of Ca<sup>2+</sup>-independent type II antifreeze protein from longsnout poacher, *Brachyopsis rostratus*. *J Mol Biol* 382:734–746
- Nutt DR, Smith JC (2008) Function of the hydration layer around an antifreeze protein revealed by atomistic molecular dynamics simulations. *J Am Chem Soc* 130:13066–13073
- Olijve LLC, Meister K, DeVries AL, Duman JG, Guo S, Bakker HJ, Voets IK (2016) Blocking rapid ice crystal growth through nonbasal plane adsorption of antifreeze proteins. *Proc Natl Acad Sci USA* 113:3740–3745
- Padilla JE, Colovos C, Yeates TO (2001) Nanohedra: using symmetry to design self assembling protein cages, layers, crystals, and filaments. *Proc Natl Acad Sci USA* 98:2217–2221
- Patel SN, Graether SP (2010) Structures and ice-binding faces of the alanine-rich type I antifreeze proteins. *Biochem Cell Biol* 88:223–229
- Pentelute BL, Gates ZP, Tereshko V, Dashnau JL, Vanderkooi JM, Kossiakoff AA, Kent SB (2008) X-ray structure of snow flea antifreeze protein determined by racemic crystallization of synthetic protein enantiomers. *J Am Chem Soc* 130:9695–9701
- Pertaya N, Celik Y, DiPrinzio CL, Wettlaufer JS, Davies PL, Braslavsky I (2007a) Growth-melt asymmetry in ice crystals under the influence of spruce budworm antifreeze protein. *J Phys Condens Matter* 19:412101
- Pertaya N, Marshall CB, DiPrinzio CL, Wilen L, Thomson ES, Wettlaufer JS, Davies PL, Braslavsky I (2007b) Fluorescence microscopy evidence for quasi-permanent attachment of antifreeze proteins to ice surfaces. *Biophys J* 92:3663–3673
- Pertaya N, Marshall CB, Celik Y, Davies PL, Braslavsky I (2008) Direct visualization of spruce budworm antifreeze protein interacting with ice crystals: basal plane affinity confers hyperactivity. *Biophys J* 95:333–341
- Phippen SW, Stevens CA, Vance TDR, King NP, Baker D, Davies PL (2016) Multivalent display of antifreeze proteins by fusion to self-assembling protein cages enhances ice-binding activities. *Biochemistry* 55:6811–6820
- Pummer BG, Budke C, Augustin-Bauditz S, Niedermeier D, Felgitsch L, Kampf CJ, Huber RG, Liedl KR, Loerting T, Moschen T et al (2015) Ice nucleation by water-soluble macromolecules. *Atmos Chem Phys* 15:4077–4091
- Qiu Y, Hudait A, Molinero V (2019) How size and aggregation of ice-binding proteins control their ice nucleation efficiency. *J Am Chem Soc* 141:7439–7452
- Raymond JA, DeVries AL (1977) Adsorption inhibition as a mechanism of freezing resistance in polar fishes. *Proc Natl Acad Sci USA* 74:2589–2593
- Raymond JA, Kim HJ (2012) Possible role of horizontal gene transfer in the colonization of sea ice by algae. *PLoS One* 7:e35968

- Sander LM, Tkachenko AV (2004) Kinetic pinning and biological antifreezes. *Phys Rev Lett* 93:128102
- Scott GK, Hayes PH, Fletcher GL, Davies PL (1988) Wolffish antifreeze protein genes are primarily organized as tandem repeats that each contain two genes in inverted orientation. *Mol Cell Biol* 8:3670–3675
- Scotter AJ, Marshall CB, Graham LA, Gilbert JA, Garnham CP, Davies PL (2006) The basis for hyperactivity of antifreeze proteins. *Cryobiology* 53:229–239
- Sicheri F, Yang DSC (1995) Ice-binding structure and mechanism of an antifreeze protein from Winter Flounder. *Nature* 375:427–431
- Smolin N, Daggett V (2008) Formation of ice-like water structure on the surface of an antifreeze protein. *J Phys Chem B* 112:6193–6202
- Sonnichsen FD, Sykes BD, Chao H, Davies PL (1993) The nonhelical structure of antifreeze protein type-iii. *Science* 259:1154–1157
- Sonnichsen FD, DeLuca CI, Davies PL, Sykes BD (1996) Refined solution structure of type III antifreeze protein: hydrophobic groups may be involved in the energetics of the protein-ice interaction. *Structure* 4:1325–1337
- Stevens CA, Drori R, Zalis S, Braslavsky I, Davies PL (2015) Dendrimer-linked antifreeze proteins have superior activity and thermal recovery. *Bioconjug Chem* 26:1908–1915
- Sun T, Lin FH, Campbell RL, Allingham JS, Davies PL (2014) An antifreeze protein folds with an interior network of more than 400 semi-clathrate waters. *Science* 343:795–798
- Sun TJ, Gauthier SY, Campbell RL, Davies PL (2015) Revealing surface waters on an antifreeze protein by fusion protein crystallography combined with molecular dynamic simulations. *J Phys Chem B* 119:12808–12815
- Tachibana Y, Fletcher GL, Fujitani N, Tsuda S, Monde K, Nishimura SI (2004) Antifreeze glycoproteins: elucidation of the structural motifs that are essential for antifreeze activity. *Angew Chem Int Ed* 43:856–862
- Takamichi M, Nishimiya Y, Miura A, Tsuda S (2007) Effect of annealing time of an ice crystal on the activity of type III antifreeze protein. *FEBS J* 274:6469–6476
- Takamichi M, Nishimiya Y, Miura A, Tsuda S (2009) Fully active QAE isoform confers thermal hysteresis activity on a defective SP isoform of type III antifreeze protein. *FEBS J* 276:1471–1479
- Vance TDR, Olijve LLC, Campbell RL, Voets IK, Davies PL, Guo S (2014) Ca<sup>2+</sup>-stabilized adhesin helps an Antarctic bacterium reach out and bind ice. *Biosci Rep* 34:e00121
- Vance TDR, Graham LA, Davies PL (2018) An ice-binding and tandem beta-sandwich domain-containing protein in *Shewanella frigidimarina* is a potential new type of ice adhesin. *FEBS J* 285:1511–1527
- Venketesh S, Dayananda C (2008) Properties, potentials, and prospects of antifreeze proteins. *Crit Rev Biotechnol* 28:57–82
- Vrielink ASO, Aloï A, Olijve LLC, Voets IK (2016) Interaction of ice binding proteins with ice, water and ions. *Biointerphases* 11:018906
- Wang X, DeVries AL, Cheng CH (1995) Antifreeze peptide heterogeneity in an Antarctic eel pout includes an unusually large major variant comprised of two 7 kDa type III AFPs linked in tandem. *Biochim Biophys Acta* 1247:163–172
- Warren G, Corotto L (1989) The consensus sequence of ice nucleation proteins from *Erwinia-Herbicola*, *Pseudomonas-Fluorescens* and *Pseudomonas-Syringae*. *Gene* 85:239–242
- Wen DY, Laursen RA (1992a) A model for binding of an antifreeze polypeptide to ice. *Biophys J* 63:1659–1662
- Wen DY, Laursen RA (1992b) Structure-function-relationships in an antifreeze polypeptide – the role of neutral, polar amino-acids. *J Biol Chem* 267:14102–14108
- Wierzbicki A, Dalal P, Cheatham Iii TE, Knickelbein JE, Haymet ADJ, Madura JD (2007) Antifreeze proteins at the ice/water interface: three calculated discriminating properties for orientation of type i proteins. *Biophys J* 93:1442–1451



- Wilkens C, Poulsen JCN, Ramløv H, Lo Leggio L (2014) Purification, crystal structure determination and functional characterization of type III antifreeze proteins from the European eelpout *Zoarces viviparus*. *Cryobiology* 69:163–168
- Wilson PW (1993) Explaining thermal hysteresis by the kelvin effect. *Cryo Letters* 14:31–36
- Wilson PW, Osterday KE, Heneghan AF, Haymet ADJ (2010) Type I antifreeze proteins enhance ice nucleation above certain concentrations. *J Biol Chem* 285:34741–34745
- Wolber P, Warren G (1989) Bacterial ice-nucleation proteins. *Trends Biochem Sci* 14:179–182
- Wu DW, Duman JG, Xu L (1991) Enhancement of insect antifreeze protein-activity by antibodies. *Biochim Biophys Acta* 1076:416–420
- Wu Y, Banoub J, Goddard SV, Kao MH, Fletcher GL (2001) Antifreeze glycoproteins: relationship between molecular weight, thermal hysteresis and the inhibition of leakage from liposomes during thermotropic phase transition. *Comp Biochem Physiol B Biochem Mol Biol* 128:265–273
- Xiao N, Suzuki K, Nishimiya Y, Kondo H, Miura A, Tsuda S, Hoshino T (2010) Comparison of functional properties of two fungal antifreeze proteins from *Antarctomyces psychrotrophicus* and *Typhula ishikariensis*. *FEBS J* 277:394–403
- Xiao N, Hanada Y, Seki H, Kondo H, Tsuda S, Hoshino T (2014) Annealing condition influences thermal hysteresis of fungal type ice-binding proteins. *Cryobiology* 68:159–161
- Yamashita Y, Miura R, Takemoto Y, Tsuda S, Kawahara H, Obata H (2003) Type II antifreeze protein from a mid-latitude freshwater fish, Japanese smelt (*Hypomesus nipponensis*). *Biosci Biotechnol Biochem* 67:461–466
- Yang C, Sharp KA (2004) The mechanism of the type III antifreeze protein action: a computational study. *Biophys Chem* 109:137–148
- Yang C, Sharp KA (2005) Hydrophobic tendency of polar group hydration as a major force in type I antifreeze protein recognition. *Proteins Struct Funct Bioinf* 59:266–274
- Yang DSC, Sax M, Chakrabarty A, Hew CL (1988) Crystal structure of an antifreeze polypeptide and its mechanistic implications. *Nature* 333:232–237
- Yang Z, Zhou Y, Liu K, Cheng Y, Liu R, Chen G, Jia Z (2003) Computational study on the function of water within a beta-helix antifreeze protein dimer and in the process of ice-protein binding. *Biophys J* 85:2599–2605
- Yeh Y, Feeney RE (1996) Antifreeze proteins: structures and mechanisms of function. *Chem Rev* 96:601–618
- Zepeda S, Yokoyama E, Uda Y, Katagiri C, Furukawa Y (2008) In situ observation of antifreeze glycoprotein kinetics at the ice interface reveals a two-step reversible adsorption mechanism. *Cryst Growth Des* 8:3666–3672
- Zhang W, Laursen RA (1998) Structure-function relationships in a type I antifreeze polypeptide – the role of threonine methyl and hydroxyl groups in antifreeze activity. *J Biol Chem* 273:34806–34812